Spring 2023

A metagenomic analysis of the microbial communities associated with different hydrothermal vent chimneys

Laura Murray
Western Washington University, lmurray0918@gmail.com

A metagenomic analysis of the microbial communities associated with different hydrothermal vent chimneys

By

Laura Murray

Accepted in Partial Completion of the
Requirements for the Degree Master of
Science

ADVISORY COMMITTEE

Dr. Craig Moyer, Chair

Dr. Dietmar Schwarz

Dr. Heather Fullerton

GRADUATE SCHOOL

David L. Patrick, Dean

Master's Thesis

In presenting this thesis in partial fulfillment of the requirements for a master's degree at Western Washington University, I grant to Western Washington University the non-exclusive royalty-free right to archive, reproduce, distribute, and display the thesis in any and all forms, including electronic format, via any digital library mechanisms maintained by WWU.

I represent and warrant this is my original work and does not infringe or violate any rights of others. I warrant that I have obtained written permission from the owner of any third party copyrighted material included in these files.

I acknowledge that I retain ownership rights to the copyright of this work, including but not limited to the right to use all or part of this work in future works, such as articles or books.

Library users are granted permission for individual, research and non-commercial reproduction of this work for educational purposes only. Any further digital posting of this document requires specific permission from the author.

Any copying or publication of this thesis for commercial purposes, or for financial gain, is not allowed without my written permission.

Laura Murray

5/3/2023

A metagenomic analysis of the microbial communities associated with different hydrothermal vent chimneys

A Thesis
Presented to
The Faculty of
Western Washington University

In Partial Fulfillment
Of the Requirements for the Degree
Master of Science

By
Laura A. Murray
May 2023

ABSTRACT

Hydrothermal vents host a diverse community of microorganisms that utilize chemical gradients from the venting fluid for their metabolisms. The venting fluid can solidify to form chimney structures that these microbes adhere to and colonize. These chimney structures are found throughout many different locations in the world's oceans. In this study, comparative metagenomic analyses of microbial communities on five chimney structures from around the Pacific Ocean were elucidated focusing on the core taxa and genes that are characteristic for each of these hydrothermal vent chimneys, as well as highlighting differences among the taxa and genes found at each chimney due to parameters such as physical characteristics, chemistry, and activity of the vents. DNA from the chimneys was sequenced, assembled into contigs, annotated for gene function, and binned into metagenome assembled genomes, or MAGs. Genes used for carbon, oxygen, sulfur, nitrogen, iron, and arsenic metabolism were found at varying abundances at each of the chimneys, largely from either Gammaproteobacteria or Campylobacteria. Many taxa had overlap of these metabolism genes, indicating that functional redundancy is critical for life at these hydrothermal vents. It was found that high relative abundance of oxygen metabolism genes coupled with low carbon fixation genes could be used as a unique identifier for inactive chimneys. Genes used for DNA repair, chemotaxis, and transposases were found to be at higher abundances at each of these hydrothermal chimneys allowing for enhanced adaptations to the ever-changing chemical and physical conditions encountered. The combination of genes detected in this study sheds light on the community structure and metabolic potential of hydrothermal vent chimneys throughout the Pacific Ocean.

ACKNOWLEDGEMENTS

I would like to thank Dr. Craig Moyer, Dr. Heather Fullerton, and Dr. Dietmar Schwarz for their help on this project as members of my committee. I would also like to thank Lindsey Smith, Amanda Stromecki, Emily Musenbrock, and Alyssa Tsukada for their insight. Finally, I would like to thank the WWU Biology Department and the WWU graduate school for the funding I received to complete this project.

Table of Contents

List of Tables and Figures

INTRODUCTION

Deep sea hydrothermal vents have been an ecosystem of interest since their discovery in 1977 (Galambos *et al.,* 2019). With their steep chemical and temperature gradients due to fluid venting up from beneath the earth's crust, chemoautotrophic microorganisms that use redox gradients for energy can find a suitable habitat. As the hot fluid is released from these vents, some of the reduced chemicals in the fluid (e.g., sulfides, iron, and manganese) mix with the oxygenated seawater and solidify to form structures known as hydrothermal vent chimneys (Opatkiewicz, *et al.*, 2009). Not only do these chimneys provide an initial surface for microbes to adhere to and colonize, but vent fluids support growth of chemoautotrophic microbes (Kato *et al.,* 2018). The metabolic byproducts of these microbes are disseminated throughout the ocean; contributing to global geochemical cycling and utilized as energy sources by macroorganisms throughout the world's oceans (Edwards, 2004; Ardyna *et al.,* 2019). Organisms that physically modify a habitat are known as "ecosystem engineers", by creating the physical structure of the hydrothermal vent chimneys, chemoautotrophic microbes enhance community richness and diversity by allowing for hydrothermal vents to become more diverse communities (Wright et al., 2002).

In addition to hydrothermal vents being ecologically important, they are also economically important, due to the high levels of valuable metals like silver, copper, cobalt, and gold that make up these chimneys (Han *et al.,* 2018). Because of the high concentration of valuable metals, these ecosystems are becoming popular sites for deep-sea mining. Deep-sea mining has been shown to produce large particle plumes and landslides that can impact benthic filter feeders' ability to access food. Mining the chimneys would also destroy the surface that microbes use to adhere to, forcing them to find other suitable habitats (Orcutt *et al.,* 2020). This could have downstream impacts since these microbes could act as settlement cues for vent-endemic invertebrates (O'Brian *et al.,*

2015). Without these microbial primary producers at these chimney sites, the rich ecosystem of larger organisms would not have access to their usual source of energy, making hydrothermal vents largely uninhabitable. The impact of deep-sea mining on the communities of both micro and macroorganisms remains largely understudied (Han *et al.,* 2018).

Vent chimneys are found worldwide and have a wide range of venting temperatures, chemical composition, and flow rates (Emerson and Moyer, 2015). Differences in the chemistry of the vents dictate the biogeographical distribution of microbes. Microbial growth is dependent on many factors, including presence of oxygen, pH, pressure, heat flux, geology, and reduced chemicals that autotrophic microbes use; due to the necessity of microbes having optimal conditions needed to enhance growth, vents with similar environmental characteristics have similar microbial communities (Dick, 2019). In this study, we seek to identify the microbial community members at each chimney, investigate the similarities and differences in microbial community structure among these selected vent chimneys, identify the common genes found at each chimney, and ask what do they imply about metabolic processes happening there? The four sampling sites in this study are all found along the plate boundary in the Pacific Ocean, known as the "Ring of Fire" (Figure 1). These sites are Magic Mountain on the southern Explorer Ridge, Axial Seamount located on the Juan de Fuca Ridge, Guaymas Basin within the Gulf of California, and the Urashima Vent Field along the Southern Mariana back-arc (Figure 1). Detailed maps of each site can be found in Tunnicliffe *et al.,* 1985 (Magic Mountain), Chadwick *et al.,* 2016 (Axial Seamount), Teske *et al.,* 2016 (Guaymas Basin), and Toki *et al.,* 2014 (Urashima). Despite differences in location, these venting sites are all sulfide-rich, with the potential for chemoautotrophy by a diverse array of microorganisms (Table 1).

Magic Mountain is a hydrothermal vent field located approximately 150 miles off the coast of Vancouver Island. This site has over 50 vents, both active and inactive, including the inactive Ochre Chimney, the site used in this analysis. The chimney structures found in this vent field are composed largely of sulfide deposits (Fortin *et al.*, 1998). While many studies have been done on the microbial communities present at active vent chimneys, little is known about the composition of inactive, weathered chimneys. Active chimneys at Magic Mountain are dominated by Campylobacteria, the class formerly known as Epsilonproteobacteria (Waite *et al.*, 2017), with similar community composition to that of Axial Seamount chimneys. When examining inactive chimneys in other locations, sulfide-oxidizing Gammaproteobacteria tend to dominate the microbial communities as they can use metal-sulfide present in the chimney structures and mineral deposits for energy (Meier *et al.,* 2018; Edwards *et al.,* 2003; Sylvan *et al.,* 2012).

Axial is found approximately 300 miles west of Oregon on the Juan de Fuca Ridge. This seamount is an active submarine volcano and a site of extensive hydrothermal venting, with the most recent eruption occurring in 2015 (Chadwick *et al,* 2016). The high volcanic activity of this caldera produces a large amount of hydrogen sulfide, ferrous oxide, and methane that are released in the vented fluid with eruption events. Many of the microbes found at this site oxidize these reduced compounds for energy (Mattes *et al.,* 2013). Therefore, the concentration of the minerals can be indicative of the time elapsed since the last eruption, as more microbes use these minerals, the more depleted they become. Sulfur-oxidizing and methanogenic microbes were identified with clone libraries for bacteria and archaea, their abundances correlating to the high concentrations of hydrogen sulfide and methane (Opatkiewicz *et al.,* 2009). Previous analyses of Axial vent plumes and microbial mats have used metagenomic analysis to understand the total metabolic potential of the community. When several subseafloor venting sites at Axial Seamount were examined, it was

determined that geochemistry and physical characteristics of the venting sites are important in shaping the community structure and genes present at each vent. Aquificae, Gammaproteobacteria, Campylobacteria, and classes of methanogenic archaea dominated the microbial communities found at these venting sites (Fortunato, *et al.,* 2018).

The Guaymas Basin spreading center located in the Gulf of California, is highly active with steep temperature gradients and is covered with a layer of a few hundred meters of organic-rich sediment. Some chimneys found in the Guaymas Basin are characterized not by direct venting but have internal hydrothermal fluid circulation due to their shape (Teske *et al.,* 2016). These unique chimneys have pagoda-like structures that force the vent fluid back down through the chimney, circulating the fluid internally, leading to large, internal temperature gradients, which allow for a diverse environment that hosts many microorganisms with many different metabolisms and temperature preferences. In a metagenomic analysis of Guaymas Basin sediments, genes for methane, hydrogen, and sulfide metabolisms were found to be enriched in hydrothermal sediments compared to background sediments (Dombrowski *et al.*, 2018). A previous metagenomic analysis of a chimney sample demonstrated that heterotrophic sulfate-reducing bacteria were found at higher abundances due to the high concentrations of hydrocarbons found in the Guaymas Basin (He *et al.,* 2015).

The Urashima Vent Field is located on the Mariana back-arc southwest of Guam. At Urashima, dissolved sulfide and hydrogen concentrations in vent effluent are enhanced. Due to the high levels of sulfide, the microbial community is dominated by Campylobacteria, which oxidize sulfide (Trembath-Reichert *et al.,* 2018). Along with Campylobacteria, the Urashima Vent Field has shown a relatively high abundance of Zetaproteobacteria, a class of iron-oxidizing bacteria that forms dense mat structures made from iron oxides and polysaccharides which are used as a

colonizing surface for other microbial taxa (McAllister *et al.,* 2020). The chimneys found along the Mariana back-arc and Magic Mountain are highly understudied regarding metagenomics, which contrasts with the initial characterizations at Guaymas Basin and Axial Seamount hydrothermal vent sites.

This study used enhanced metagenomic analyses to compare the associated microbial communities of hydrothermal vent chimneys across the Pacific Ocean, and to determine similarities or differences in the metabolic potential of these microbial communities. This metagenomic analysis approach has made a more detailed characterization of metabolic pathways and diversity within these hydrothermal vent microbial communities possible. Microbial communities that reside in hydrothermal vent chimneys were primarily found to use chemoautotrophic metabolisms. Some taxa may have varied metabolisms that allow them to reside at all chimney locations, while some may be metabolically restrictive depending on the chemical composition of that chimney. Because of this, the types of microorganisms that reside in the chimneys as well as their metabolic potential may be dictated by the reduced compounds available to them.

METHODS

Study Sites and Sampling

Chimneys were collected from (1) Axial Seamount, (2) Magic Mountain, (3) Guaymas Basin, and (4) two chimneys from the Urashima Vent Field along the Mariana back-arc using either a self-sealing scoop sampler or by using robotic arm to place dislodged chimney pieces directly into a hinged box that could be sealed off prior to ROV/submersible ascent. Both hinged box and scoop samplers were constructed from PVC. At Axial Seamount along the Juan de Fuca Ridge, Castle Chimney was collected on August 4th, 2002 with ROV ROPOS aboard the R/V Thomas G. Thompson. The Ochre Chimney at Magic Mountain Vent Field along the southern Explorer Ridge was collected on July 29th, 2002 with ROV ROPOS aboard the R/V Thomas G. Thompson. The Pagoda Chimney at the Guaymas Basin Vent Field was collected on October 7th, 1994 with HOV ALVIN aboard the R/V Atlantis. Two chimney samples, Snap-Snap and Ultra-No-Chi-Chi, were collected with ROV Jason aboard the R/V Roger Revelle from the Urashima Vent Field, along the Mariana back-arc on the western side of the Pacific Ocean. Snap-Snap Chimney was sampled on November 1st, 2014 and Ultra-No-Chi-Chi Chimney was sampled on December 18th, 2014. All chimney samples from all sites were immediately preserved with RNAlater, then stored at -80°C until DNA could be extracted in the laboratory.

Metagenomic Extraction and Sequencing

The DNA of each of the five chimney samples was extracted using the protocol from the DNeasy Power Soil Kit (Qiagen, Hilden, Germany). The extracted DNA was separated by electrophoresis to only include strands greater than 1 kb in size using an Aurora System (Boreal Genomics, Vancouver, BC). Nextera indices were added to purified DNA fragments per the manufacturer's protocol (Illumina, San Diego, CA). The indexed fragments were purified using

AMPure XP Beads according to manufacturer's protocol (Beckman Coulter, IN). The library was quantified with a Qubit 2.0 fluorometer (ThermoFisher, MA) and sequenced on the Illumina MiSeq sequencer with v3.0 chemistry to generate 2x300 bp paired-end reads at Shannon Point Marine Center, WWU.

Sequence Analysis

QC of reads

After sequencing, the reads were assessed and trimmed for quality control using the program Trimmomatic v.0.40 (Bolger *et al.,* 2014). This trimming removed any sequencing reads that are less than a phred quality score of 25. The reads were assessed for final quality, as well as GC content and adapter content using the program FastQC v.0.11.9 (Andrews, 2010).

Assembly

All metagenomic analyses were done under the general metagenomic pipeline, SqueezeMeta v.1.5.1 (Tamames and Puente-Sanchez, 2019) under co-assembly mode using default parameters and a minimum contig length of 200 base pairs. Once the reads were trimmed for quality, they were assembled into contigs using the program MegaHIT with a minimum contig length of 200 base pairs (Li *et al.,* 2015). This program uses de Bruijn graph algorithms to construct the sequence reads into contigs which then can be further analyzed for gene presence and functional annotation. The assembled contigs were checked for N50 values, which represents the sequence length of the shortest contig at 50% of the total assembly length, as well as rough taxonomy using the program MetaQuast (Mikheenko *et al.*, 2016). The genes of the assembled contigs from the output of MegaHIT were predicted using the program Prodigal (Hyatt *et al.,* 2010). Small subunit (SSU) rRNA genes were pulled from the assembled contigs using Barrnap (Seeman, 2014) and classified using the RDP naïve Bayesian classifier (Wang *et al.,* 2007).

Functional annotation and taxonomic assignment of genes

Gene sequences were compared for homology using Diamond v.2.7.14 (Buchfink *et al*., 2021). Diamond compared against three databases: GenBank nr with an LCA algorithm for taxonomy, the eggNOG database for COG annotation, and the KEGG database for KEGG annotation at the nucleotide level. The KEGG genes were then functionally and taxonomically assigned using SqueezeMeta. Bowtie2 v.2.4.5 was used to estimate coverage and abundance of each gene and contig (Langmead and Salzberg, 2012). Gene abundances were calculated using STAMP (Parks *et al.*, 2015), then percent relative abundance of each gene was calculated by taking the raw read counts for each ORF, dividing it by the total reads in the sample, and multiplying by 100. Coverage values (bases mapped/ORF length) and normalized RPKM values were calculated using custom SqueezeMeta pipeline scripts. All outputs of taxonomic names present in this analysis reflect the names in the databases at the time of assembly and assignment. Contig assemblies were loaded into FeGenie to evaluate the abundance of different iron genes in each chimney (Garber *et al.,* 2020). Outputs were visualized using a stacked bar graph made in R with the package ggplot2 v.3.3.5 (Wickham, 2016).

Binning

After assembly, the contigs were binned into metagenomic assembled genomes, or MAGs, twice using Metabat2 v.2.15 (Kang *et al.,* 2019) and Maxbin2 v.2.2.7 (Wu *et al.,* 2015). The outputs of both binning programs were merged using DAStool v.1.1.3 (Sieber *et al.,* 2018). The bins were checked for completeness and contamination using the program CheckM v.1.1.3 (Parks *et al.,* 2015), then taxonomically assigned using the same LCA algorithm in SqueezeMeta as the taxonomic assignment of the genes above.

Data analysis

In R v.3.6.3, the results of the SqueezeMeta co-assembly pipeline were imported using the R package SQMtools v.0.7.0 (Puente-Sanchez *et al.,* 2020). This package was used to plot taxonomy of contigs, functional profiles of the genes and contigs, and MAG information. The R package, vegan (Oksanen *et al.,* 2008) was used to determine permutational multivariate analysis of variance (PERMANOVA) among the five chimneys with 999 permutations and Bray-Curtis distance method, non-metric multidimensional scaling (NMDS) based on Bray-Curtis distance of KEGG functions, and relative abundance and diversity of the taxa found at each chimney using the Simpson index. The similarity of taxa found at each chimney was analyzed using Bray Curtis distance matrix and visualized with a dendrogram plot made in vegan. The R package ggplot2 was used to visualize relative abundance of ORFs at each chimney by creating heatmaps and bubble plots.

RESULTS

Assembly

In order to evaluate the connection between microbes' metabolic potential and biogeochemical cycling at hydrothermal vent chimneys, five different chimneys from around the Pacific Ocean were sampled and analyzed for their metagenomic composition: Castle Chimney from the Axial Seamount on the Juan de Fuca Ridge, the inactive Ochre Chimney from the Magic Mountain Vent Field along the southern Explorer Ridge, Pagoda Chimney from the Guaymas Basin, and Snap-Snap and Ultra-No-Chi-Chi Chimneys from Urashima Vent Field along the Mariana back-arc (Figure 1, 2). After sequencing and filtration for quality, 207,450,568 reads were assembled into 15,601,568 contigs. The average contig length and N50 was 385 base pairs. Average coverage of contigs was 0.669 at Ochre, 0.815 at Castle, 0.515 at Pagoda, 0.388 at Snap, and 0.446 at Ultra. Of those contigs, 23,040 were mapped to SSU rRNA genes. The composite assembly resulted in 43 MAGs from five metagenomes were selected after binning and used in downstream analysis (Supp. Table 1). Of the 43 MAGs selected, the completeness ranged from 52% to 10%, with a contamination range between 0% to 4.76% (Supp. Table 1). Due to low completeness and high level of contamination within some of the MAGs, further analysis was done directly on the assembled contigs.

ORF Abundances

After composite assembly, a total of 17,978,241 ORFs were identified and of these 40.7% were able to be annotated. Castle Chimney had 4,104,828 ORFs with 1,396,906 KEGG annotations, with 34% of its reads annotated. Pagoda Chimney had 3,839,549 ORFs with 1,454,544 KEGG annotations, leading to 37.9% of reads annotated. Snap-Snap Chimney had 2,464,387 ORFs with 1,189,805 KEGG annotations, making 48.3% of its reads annotated. Ultra-

No-Chi-Chi Chimney had 2,371,834 ORFs with 1,089,836 KEGG annotations, or 45.9% of reads annotated. The Ochre Chimney had 5,197,643 ORFs with 2,181,421 KEGG annotations, with 42% of its reads annotated.

PERMANOVA Analysis and Similarity Matrices

All five chimneys were distinctly separated in the NMDS plot, indicating unique environmental parameters at each chimney (Figure 3A). Clustering of samples using Bray-Curtis distance matrices and NMDS plot of KEGG gene functions showed the inactive Ochre Chimney further separated from the other chimney samples and that the two Urashima chimneys cluster closest together (Figure 3A). When clustered by taxa, Pagoda Chimney clustered as an outgroup, while the two Urashima chimneys clustered most closely together, and the Castle and Ochre chimneys also clustered together (Figure 3B). Despite each chimney having an R squared value above the significance threshold for each variable after PERMANOVA analysis, the p-value for each of the variables was 0.1 or greater, likely due to each chimney only having a single sample. Therefore, analysis of variance of these variables on each chimney was unable to be determined.

Taxonomy

To visualize the taxonomic assignment of ORFs for each chimney, the top 15 most abundant microbial classes were plotted for each sample (Figure 4A). The Castle Chimney community was made up of 38% unclassified Bacteria and 38% Gammaproteobacteria, with 15% unclassified Proteobacteria, which were recently reclassified as Pseudomonadota (Oren and Garrity, 2021), with less than 10% Alphaproteobacteria, unclassified Bacteroidetes, and Deltaproteobacteria. Pagoda Chimney was found to be comprised of 30% unclassified Bacteria and 21% unclassified Bacteroidetes, with 10% Campylobacteria, 10% unclassified Chloroflexi 9% Deltaproteobacteria, and 5% Methanopyri. Both Urashima Chimneys, Snap-Snap and Ultra-No-

Chi-Chi had similar distributions of microbial classes. These chimneys were dominated by 54% and 48% Campylobacteria respectively, followed by 8% and 10% unclassified Bacteria, 10% and 7% unclassified Proteobacteria, 8% and 11% Alphaproteobacteria, and 8% and 12% Zetaproteobacteria, respectively. Snap-Snap Chimney, the slightly cooler and shallower chimney of the two, had a larger percentage of Campylobacteria and Deltaproteobacteria than the Ultra-No-Chi-Chi Chimney. The Ochre Chimney showed a similar distribution to the Castle Chimney, with 26% unclassified Bacteria, 18% Gammaproteobacteria, 12% unclassified Proteobacteria, 21% Alphaproteobacteria, and 11% unclassified Chloroflexi.

SSU rRNA gene sequences were extracted from the chimney metagenomes and evaluated for taxonomy (Figure 4B). Of these, 4596 rRNA sequences were mapped to the Castle Chimney, 8918 were mapped to the Pagoda Chimney, 8425 were mapped to Snap-Snap Chimney, 9347 were mapped to Ultra-No-Chi-Chi Chimney, and 5202 were mapped to the Ochre Chimney. The sequences were assigned to 342 different taxa ranging from genus to superkingdom. Of these, the most abundant taxa in all chimneys were Bacteria, with 5494 SSU genes identified, Proteobacteria, with 845 SSU genes identified, Gammaproteobacteria, with 683 SSU genes identified, *Sulfurovum*, with 655 SSU genes identified, and Bacteroidetes, with 569 SSU genes identified. Shannon diversity indices showed Pagoda Chimney with the highest alpha diversity (2.818), followed by Ultra-No-Chi-Chi Chimney (2.510), Ochre Chimney (2.161), Snap-Snap Chimney (2.143), and Castle Chimney with the lowest at 2.131 (data not shown).

Gene Abundances

The top 15 most abundant genes based on KEGG assignment were identified for each chimney. The most abundant gene present in all chimneys was a putative transposase gene (Figure 5). Notably, an ammonium transporter gene was also present in the top 15 most abundant

genes, with higher abundance at Castle Chimney and lower abundance at the Pagoda Chimney. DNA-directed RNA polymerase was present at all chimneys, with higher abundances in Ochre and Pagoda. Two chemotaxis genes were found at high abundance in the Snap-Snap Chimney but less abundant in the other chimneys.

In each chimney, the top five most abundant annotated genes were identified and interestingly there was no overlap in function. In the Castle Chimney, an RNA-directed DNA polymerase gene (*itrA*) was the most abundant gene with 13,937 reads, an intracellular multiplication protein (*icmB*) had 11,147 reads, a type I restriction enzyme gene (*hsdR*) had 10,355 reads, a heavy metal exporter gene (*czcA*) had 10,152 reads, and an insecticidal toxin complex protein (*tccC*) had 8,344 reads mapped. The top five genes identified at Pagoda Chimney were a NADH-ubiquinone oxidoreductase chain 5 gene (*ndh5*) with 6,041 reads, an NADH-ubiquinone oxidoreductase chain 4 gene (*ndh4*) with 5,792 reads, a cytochrome c oxidase gene (*aa3*) with 5,363 reads, a ubiquinol-cytochrome c reductase gene (*cytB*) with 4,526 reads, and an NADH-ubiquinone oxidoreductase chain 2 gene (*ndh2*) with 3,312 reads mapped. The top five most abundant genes in the Snap-Snap Chimney were serralysin (*prtC*) with 5,487 reads, aconitate hydratase (*acnA*) with 4,421 reads, DNA polymerase I (*polA*) with 4,148 reads, periplasmic nitrate reductase (*napA*) with 4,125 reads, and cobalt-zinc-cadmium resistance protein (*czcA*) with 4,022 reads mapped. In the Ultra-No-Chi-Chi Chimney, the top five genes were serine/threonine protein kinase with 9,257 reads, Ca-activated chloride channel homolog (*yfbK*) with 8,855 reads, O-antigen biosynthesis protein (*rfbC*) with 7,444 reads, penicillin binding protein (*mrcA*) with 6,960 reads, and sensor histidine kinase (*varS*) 6,368 reads mapped. In the Ochre Chimney, the top genes were ryanodine receptor 2 (*ryr2*) with 2,281 reads, DNA repair protein (*radC*) with 1,621 reads, ribonucleoside-triphosphate reductase (formate) (*nrdD*) with 1,029 reads, 7,8-dihydro-6-

hydroxymethylpterin dimethyltransferase with 949 reads, and DNA directed RNA polymerase I (*rpoA1*) with 902 reads mapped.

Metabolic potential

Carbon cycling

Chemosynthetic primary producers at hydrothermal vent chimneys have been shown to fix carbon via a number of pathways, including the reverse tricarboxylic acid cycle (rTCA), the Calvin-Benson-Bassham (CBB) cycle, and the Wood-Ljungdahl (WL) pathway. The rTCA cycle uses the enzyme ATP citrate lyase (*aclB)* to take CO_2 and water to make carbon compounds that can be used for energy by microorganisms in low oxygen environments. The *aclB* gene was found to be present in all five chimneys, indicating that carbon fixation via the rTCA cycle could be occurring. The Castle Chimney and Ochre Chimney both had *aclB* genes identified as belonging to Nitrospirae and Campylobacteria (Supp. Tables 2 and 3). At the Pagoda Chimney, *aclB* was found in unclassified archaea and bacteria, as well as Thermoplasmata, Candidatus Bipolaricaulota, Chloroflexi, Aquificae, and Campylobacteria. At the Urashima Chimneys, Snap-Snap, and Ultra-No-Chi-Chi, Campylobacteria *aclB* genes dominated in relative abundance (Supp. Tables 4-6).

The CBB cycle, uses the enzyme RuBisCO to fix CO_2 either with or without the presence of oxygen. The CBB cycle was identified using the RuBisCO protein, shown here by the presence of long chain and short chain RuBisCO genes, *rbcL* and *rbcS.* These genes were found to be present to a varying degree at all five chimneys, with *rbcL* dominating (Figure 6). The *rbcL* ORFs found were assigned to Alphaproteobacteria, Chloroflexi, Proteobacteria and Gammaproteobacteria taxa across all five chimneys (Figure 6, Supp. Tables 2-6). The Castle and Ochre Chimneys showed similar assignments of rbcL-assigned taxa, with Proteobacteria dominating and a low presence of

archaeal *rbcL* genes (Supp. Tables 2 and 3). In contrast, Pagoda Chimney and both Urashima chimneys showed a higher presence of archaeal *rbcL* genes (Table 2, Supp. Tables 4-6). In contrast, the *rbcS* gene was identified as unclassified Bacteria in four of the chimneys and in the Ultra-No-Chi-Chi Chimney, a small percentage of reads were assigned to Calditrichae (Supp. Table 6).

The Wood-Ljungdahl pathway reduces CO_2 to carbon monoxide using the enzyme carbon monoxide dehydrogenase (*cooS* and *acsA,* both represented here by *cooS*), and then creates acetyl-CoA using acetyl-CoA synthase (Ragsdale and Pierce, 2008). These carbon fixation pathways are important for establishing diverse microbial communities at hydrothermal vent chimneys where oxygen and organic material are lacking. The Wood-Ljungdhal pathway was found to be present across all five chimneys by presence of the *cooS* gene (Figure 6). This gene was least abundant at Ochre Chimney, and most abundant at Pagoda Chimney (Figure 6). Deltaproteobacteria, Gammaproteobacteria, and Nitrospirae identified *cooS* all were found at higher relative abundances at Castle Chimney, Chloroflexi, Deltaproteobacteria, and Methanopyri *cooS* were the most abundant at Pagoda Chimney, and Deltaproteobacteria and Nitrospirae *cooS* were found to be in the highest relative abundance at the two Urashima chimneys (Supp. Tables 2-6).

Nitrogen cycling

Three nitrogen cycling genes were annotated and taxonomically assigned for each chimney: methane/ammonia monooxygenase subunit A (*amoA*), a gene responsible for oxidizing ammonia into nitrite in the nitrification pathways, nitrogenase iron protein (*nifH*), which fixes dinitrogen to ammonia, and nitrate reductase (*nirK*), a gene responsible for the denitrification of nitrite to nitric oxide (NO). Also found to be present across all five chimneys was an ammonium

transport gene (*amt*), with the highest relative abundance in Castle Chimney and the lowest in Pagoda Chimney (Figure 5).

The least abundant nitrogen cycling gene across all five chimneys was *amoA* (Supp. Tables 2-6). Nitrification as represented by the *amoA* gene showed the greatest representation in the Ochre Chimney, with corresponding taxa including Betaproteobacteria, Deltaproteobacteria, Gammaproteobacteria, and Nitrososphaeria, unclassified Thaumarchaeota and unclassified Archaea (Supp. Table 2).

Pagoda Chimney had the lowest total abundance of nitrogen metabolism genes, but dinitrogen fixation to ammonia as represented by *nifH* was dominated by Methanopyri, Nitrospirae, Firmicutes, Gammaproteobacteria and Deltaproteobacteria (Figure 6, Supp. Table 4). Most of the ORFs assigned to *nifH* genes were found to be associated with Methanopyri, a class of methanogenic Euryarchaeota that are likely nitrogen fixers. The Castle Chimney also had a large proportion of *nifH* genes assigned to several taxa, mostly dominated by Proteobacteria, while the two Urashima chimneys had small abundances of *nifH* genes identified as Deltaproteobacteria, Thermodesulfobacteria, and Archaeoglobi (Supp. Tables 2, 5, 6).

The most prevalent form of nitrogen metabolism across the samples except the Pagoda and Castle Chimneys was denitrification via *nirK* (Figure 6). Each chimney had a unique taxonomic distribution of *nirK* taxa, with high relative abundances in Bacteroidetes, Gammaproteobacteria, and unclassified Bacteria. Ochre Chimney had the highest diversity of *nirK* genes across both archaea and bacteria, with most of the reads assigned to Nitrososphaeria (Supp. Tables 2-6).

Sulfur cycling

Two sulfur cycling genes were examined in all five chimneys: dissimilatory sulfite reductase *dsrAB,* which either catalyzes the reduction of sulfite to sulfide during the anaerobic

respiration of sulfate or acts in reverse during the oxidation of sulfide to sulfite, and thiosulfotransferase *soxAB*, which facilitates thiosulfate oxidation. Across all five chimneys, *dsrAB* was found present in Alphaproteobacteria, Deltaproteobacteria, Gammaproteobacteria, Proteobacteria, and unclassified Bacteria. It was also found in the four active chimneys as Acidobacteria and Nitrospirae. The *soxAB* genes were represented across similar taxa as *dsrAB* genes in all five chimneys. Alphaproteobacteria, Gammaproteobacteria, and unclassified Bacteria *dsrAB* genes were present in all chimneys and Deltaproteobacteria and Campylobacteria were present in the four active chimneys (Supp. Tables 2-6).

Iron cycling

To observe iron metabolisms in the chimneys, the iron oxidase gene *cyc2,* was annotated and assigned to different taxa. It is useful as an indicator of microbial iron oxidation as an energy source. The iron complex outer membrane receptor protein gene, involved in the acquisition and uptake of iron, was found to be present across all five chimneys, with the largest relative abundance found in the Snap-Snap Chimney (Figure 5). The presence of iron was confirmed at the Castle Chimney and two Urashima chimneys (Table 1). However, *cyc2* genes were found present in both the Pagoda Chimney and the Ochre Chimney. The most abundant *cyc2* gene taxon was Gammaproteobacteria, found in all chimneys except for Ultra-No-Chi-Chi (Supp. Tables 2-6). At Snap-Snap Chimney Alphaproteobacteria, Gammaproteobacteria, Bacteroidetes, and unclassified Bacteria had the *cyc2* gene. In contrast, Ultra-No-Chi-Chi only had ORFs assigned to Proteobacteria and Aquificae *cyc2* genes (Supp. Tables 2-6).

Different iron metabolic genes and gene families were also identified for each chimney using FeGenie (Supp. Fig. 1). Across all five chimneys, reads assigned to iron gene regulation dominated, with the highest percentage found in Ochre Chimney and the least in Castle Chimney.

The most reads for iron oxidation were found in Castle Chimney (Supp. Fig. 1). The prevalence of microbial iron oxidation at Castle Chimney is further evidenced by the high abundance of *cyc2* genes found at that chimney (Figure 6).

Arsenic metabolism

Arsenate reductase, *arsC,* allows for the reduction of arsenate as a method of obtaining energy and detoxification. Each of the five chimneys contained the *arsC* gene in at least 12 different taxa including Gammaproteobacteria, Bacteroidetes, Proteobacteria, and unclassified Bacteria (Supp. Tables 2-6). All five chimneys had arsenic metabolism genes present (Figure 5). Ultra-No-Chi-Chi Chimney had the most *arsC* genes present. In the Castle and Ochre chimneys, Gammaproteobacteria had the most ORFs assigned, while Campylobacteria dominated in the two Urashima chimneys. The Pagoda Chimney had the largest abundance of reads map to Bacteroidetes *arsC* genes (Supp. Tables 2-6).

Oxygen metabolism

To examine the potential for aerobic respiration at each of the chimneys, the relative abundance of two cytochrome c oxidase genes (*ccoNO* and *coxAB*) was evaluated. The *ccoNO* gene encodes a cbb_3-type cytochrome c oxidase subunit I/II, which has a high affinity for oxygen and is more prevalent in lower oxygen concentrations, while the *coxAB* gene encodes an aa_3-type cytochrome c oxidase subunit I/II, which has a low affinity for oxygen and is more prevalent in higher oxygen concentrations (de Geir, *et al.,* 1996). It was found that the *ccoNO* gene was more abundant at the Urashima chimneys as well as the Pagoda Chimney, with the least amount detected at the Castle and Ochre chimneys (Figure 6). At Ochre Chimney, Bacteriodetes, Flavobacteriia, and Gemmatimondetes had the highest relative abundance of orfs assigned to *ccoNO* genes (Supp. Table 2). Castle Chimney had a large abundance of Bacteroidetes and Gammaproteobacteria

ccoNO genes (Supp. Table 3). Chlorobi, Flavobacteriia, Bacteriodetes, and Cytophagia *ccoNO* genes were most abundant at Pagoda Chimney (Supp. Table 4). At Snap-Snap; Acidobacteria, Bacteriodetes, Chlorobi, and Flavobacteriia had the most *ccoNO* genes assigned (Supp. Table 5). Ultra-No-Chi-Chi had a similar abundance of *ccoNO* genes, with the addition of Deltaproteobacteria having a large relative abundance (Supp. Table 6). Overall, the *coxAB* gene was much higher than the *ccoNO* genes at all chimneys except Pagoda. The *coxAB* gene was least abundant at Pagoda Chimney, with a relatively high abundance at the two Urashima chimneys. There were large relative abundances of *coxAB* genes assigned in Alpha and Gammaproteobacteria in all the chimneys, and Pagoda and Ultra-No-Chi-Chi chimneys had a large relative abundance of Campylobacteria assigned to *coxAB* genes (Supp. Table 2-6).

DISCUSSION

The analysis of the metagenomics from five hydrothermal vent chimneys around the Pacific Ocean demonstrates a set of functional core genes that all the locations share while also elucidating the differences each chimney has with respect to distinct community composition and metabolic potential. After examining the binned MAGs in each chimney, the SSU rRNA taxonomic community compositions, and some common genes for carbon fixation, nitrogen, sulfur, iron, arsenic, and oxygen metabolism, each of the chimneys were found to have a distinct metabolic profile.

PERMANOVA analysis showed no statistical significance to the chimneys clustering based on geographic location, activity, depth, or temperature; however, this is likely due to having no sample replicates. Despite a lack of statistically significant data, each chimney site has a unique community of microbes. However, there were noticeable trends among certain chimneys. Similarities between Snap-Snap and Ultra-No-Chi-Chi chimneys are likely due to them being close in proximity and with similar chemical profiles. Similarities in metabolic gene presence and high prevalence of Gammaproteobacteria between Castle Chimney and Ochre Chimney likely are due to Castle Chimney being at such a shallow depth, with more oxygen for aerobic microorganisms, and Ochre Chimney has more oxygen due to the inactivity of the chimney. This is evidenced by the high relative abundance of the *coxAB* genes, indicating aerobic respiration is occurring in the presence of high oxygen (Zhou *et al.,* 2013).

The relative abundance of transposase genes in all five chimneys indicates horizontal gene transfer as a likely method of adaptation to the extreme environments of the hydrothermal vent chimneys (Reznikoff, 2003). Previous analyses have shown a higher relative abundance of transposases at hydrothermal vent chimneys compared to other microbial communities. Horizontal

gene transfer among microbial taxa increases the phenotypic diversity of the chimney communities for microbes to better respond and adapt to environmental gradients (Brazelton and Baross, 2009). This is evident when examining extremophile organisms that commonly reside at hydrothermal vents. For example, transposases as indicators of horizontal gene transfer have been shown to be common in thermophilic microbes, as demonstrated with the representative bacteria *Fervidobacterium* (Cuecas *et al.*, 2017).

The presence of an ammonia transport gene supports the high instance of ammonia oxidation at each of these chimneys, with the most found at Castle Chimney and the least at Pagoda Chimney. This is confirmed by the high abundance of archaeal *nirK* ammonia oxidation genes found at Castle Chimney, demonstrating that this chimney is likely dominated by ammonia-oxidizing archaea. A high relative abundance of ammonia transport genes was also found in the metagenomes of microbial mats at Kamaʻehuakanaloa Seamount, a location known for its high ferrous iron and ammonium concentrations (Jesser *et al.,* 2015). The ubiquity of ammonia transport genes across the chimneys suggests that like Kamaʻehuakanaloa, the microbes are accessing environmental nitrogen for assimilative or dissimilative processes (Sylvan *et al.*, 2017).

Since no geochemical data were taken to assess the arsenic concentrations at any of the sites, inferences based on presence of the *arsC* gene can provide insight into arsenic cycling at each chimney. Nine different classes of bacteria have *arsC* genes. Previous analyses have found that a diverse number of microbes can metabolize arsenic using *arsC* (Meyer-Dombard *et al.*, 2012). Since many different taxa have an arsenic reductase gene, this indicates the prevalence of arsenic and the need to detoxify it. This could indicate that arsenic is universal to chimneys and their potential venting fluids.

Ochre Chimney

Ochre Chimney is an inactive, weathered chimney; therefore, the microbial community must gain its energy from metabolism of solid minerals found in the chimney itself rather than the venting fluid present in an active chimney. The lack of venting fluid at inactive chimneys allows for more stable metabolic activity and cooler temperatures (Pan *et al.,* 2022). At Ochre Chimney, this is indicated by the lower abundance of Type I restriction enzyme and chemotaxis protein genes. The lower relative abundance of these genes suggests a lower demand for microbes to respond quickly to changing environmental gradients, such as oxygen or sulfide, as the sources of energy are limited to the chimney sediment with little fluctuation (Xie *et al.,* 2011).

Microbes at Ochre Chimney appear to largely fix carbon via the CBB cycle, with a higher prevalence of RuBisCO genes as compared to *aclB* abundance. The distribution of *rbcL* and *rbcS* assigned taxa at Ochre Chimney, dominated by Proteobacterial classes, confirms carbon cycling at inactive chimneys is done via the CBB cycle (Meier *et al.,* 2019). Other studies examining the metabolic potential of inactive hydrothermal vent chimneys on the East Pacific Rise have identified autotrophic Gammaproteobacteria using the oxidation of metal sulfides or iron oxidation coupled with nitrate reduction to fix carbon through the CBB cycle (Hou *et al.,* 2020). Notably, Ochre also has two archaeal classes assigned to *rbcL*, one in the Thaumarchaeota phylum and one at the unclassified Archaeal level. Archaeal RuBisCO genes are putatively involved in carbon dioxide fixation or AMP and nucleotide scavenging pathways (Beam *et al.,* 2014). Thaumarchaeota, specifically Nitrososphaeria, are known to be common in inactive chimneys and can metabolize low concentrations of nitrogen and carbon (Han *et al.,* 2018).

As *nirK* is largely used in archaea for ammonia oxidation and in bacteria for denitrification of nitrite, the relatively high number of different taxa that have a *nirK* gene for denitrification

indicates an abundance of nitrite as an electron donor for lithotrophic growth (Kerou *et al.,* 2016). Due to the abundance of *nirK*, it is likely that both ammonia oxidation and denitrification are occurring in this chimney. At hydrothermal vents of Explorer Ridge, nitrate was found to be more prevalent than nitrite, which explained the high relative abundance of *nirK* as compared to *nifH* (Tunnicliffe *et al.,* 1985). The lack of vent fluid flow at Ochre Chimney facilitated a change in metabolic activity, switching from a community of nitrogen fixers to a community dominated by denitrification and ammonia oxidation. This metabolic plasticity has been demonstrated in other inactive hydrothermal vent chimneys and is necessary for the survival of organisms in an ephemeral environment (Pan *et al.,* 2022).

The relatively large abundance of *amoA* genes could be due to an increased amount of ammonium found at the inactive chimney as organisms die there and organic matter is broken down (Li *et al.,* 2014). Both bacterial and archaeal *amoA* were identified and are likely critical in the nitrification process at Ochre Chimney.

The availability of sulfur is a distinguishing factor in community composition between inactive and active chimneys (Han *et al.,* 2018). Since there is no data on the hydrogen sulfide concentrations at Ochre Chimney, the presence of different sulfur compounds can only be inferred by the presence of the sulfur metabolism genes. The Gammaproteobacterial and Alphaproteobacterial *dsrAB* genes found present in Ochre Chimney are the oxidative version of *dsrAB,* indicating that these organisms are sulfur-oxidizing bacteria (Muller *et al.,* 2015). Sulfate reduction by Deltaproteobacteria present in Ochre Chimney has been found to dominate inactive chimneys, which in turn can change the mineral composition of the chimney with the production of pyrite (Han *et al.,* 2018). There was taxonomic identification overlap with *dsrAB* and *soxAB*, indicating that if dissimilatory sulfate reduction is occurring, thiosulfate oxidation could be

occurring concurrently in the same taxa. This type of functional redundancy has been shown to increase ecological stability and resilience to disturbance, like the inactivation of a chimney (Biggs *et al.,* 2020).

The relatively low abundance of *cyc2* genes assigned to Gammaproteobacteria at Ochre Chimney indicates that iron oxidation may not be as prevalent at this location or in inactive, weathered chimney structures. However, the high proportion of iron gene regulator genes and low proportion of iron transport genes as compared to the other chimneys demonstrates that iron is likely present but might only be used in assimilatory processes. Gammaproteobacteria have been shown to be primary colonizers of inactive chimneys, as they can oxidize sulfur present in the chimney structure (Hou *et al.,* 2020). These Gammaproteobacteria may act as a catalyst in the weathering of inactive iron-sulfide chimneys, which could indicate that the Ochre Chimney was towards the end of the weathering process. In addition, Gammaproteobacteria are likely actively interacting with the surface of the chimneys, as evidenced by their cytochrome c genes, sulfur oxidation genes, and carbon fixation via the CBB cycle (Meier *et al.,* 2019).

Previous analyses of oxygen tolerance of microbes at different hydrothermal vent sites have shown that Gammaproteobacteria tend to favor environments with higher oxygen (Zhou *et al.,* 2022). Ochre Chimney does have a large relative abundance of Gammaproteobacteria, as well as a very small relative abundance of *ccoNO* cytochrome c oxidase genes, further confirming the high oxygen concentrations at this chimney.

Castle Chimney

The main pathway for carbon fixation at Castle Chimney is via the CBB cycle, with most *rbcL* genes associated with different Proteobacterial classes and low relative abundances of *aclB* genes. In another analysis of Axial Seamount chimney metagenomics, Gammaproteobacteria were

found to be the largest contributing taxon for the CBB cycle for carbon fixation (Fortunato *et al.,* 2018). Gammaproteobacteria tend to favor environments with higher oxygen and lower concentrations of sulfide, making them more adept for carbon fixation via the CBB cycle (Assié *et al.,* 2020). The higher concentration of oxygen present at Castle Chimney may account for the high relative abundance of Gammaproteobacterial *rbcL* genes. The presumed high concentration of oxygen is also evidenced by the relatively low abundance of *ccoNO* genes.

Despite the abundance of rbcL, the Campylobacteria and Nitrospirae fix carbon via the rTCA cycle at Castle Chimney, which is supported by previous research at Axial Seamount (Fortunato *et al*., 2018). Campylobacteria are commonly found in environments with lower oxygen levels and higher concentrations of sulfide (Assié *et al.,* 2020). rTCA is favored over CBB in oxygen-limited environments (Oulas *et al.,* 2016), which could explain the higher relative abundance of Gammaproteobacterial CBB cycling genes over Campybacterial rTCA cycling genes.

The domination of denitrification as evidenced by the large proportion of bacterial and archaeal *nirK* genes is supported by Fortunato *et al.,* (2018), which classified *nirK* transcripts to Thaumarchaeota and other ammonia-oxidizing archaea at Axial Seamount. Organisms that had the ammonia oxidation gene, *amoA,* always had *nirK* genes as well. This indicates that these pathways are likely co-occurring in ammonia-oxidizing archaea which is hypothesized to be due to the decentralization of gene expression to maintain genetic diversity in variable environments like hydrothermal vent chimneys (Carini *et al.,* 2018).

Since Castle Chimney has nitrite reduction genes and sulfur oxidation genes present that were identified as Gammaproteobacteria, this coupled reaction is likely being performed by anaerobic sulfide-oxidizing bacteria. As with Gammaproteobacterial sulfide oxidation via *dsrAB*,

it has been shown that some Alphaproteobacteria couple denitrification via *nirK* with thiosulfate oxidation via *soxAB* in deep subsurface environments (Bell *et al.,* 2020). This appears to be true in the Castle Chimney, with both of these genes mapping to Alphaproteobacteria. Since many of these metabolic pathways have been shown to co-occur, it demonstrates that the microbes present in Castle Chimney likely may be capable of gaining electrons from several different sources.

Castle Chimney iron oxidation is dominated by Gammaproteobacteria, a class that has been previously identified on the Juan de Fuca Ridge (Edwards *et al.,* 2003). Zetaproteobacteria, an iron-oxidizing bacteria commonly found at hydrothermal vents, is notably absent in Castle Chimney. This could be due to misidentification, or the higher temperature and lower abundance of iron at Castle could influence a higher proportion of Gammaproteobacterial iron oxidation rather than Zetaproteobacterial iron oxidation, as Zetas tend to prefer lower temperatures (Mori *et al.,* 2017).

Pagoda Chimney

Shaped like a mushroom or a Pagoda topped with a domed cap and many flanges coming out of the trunk, Pagoda Chimney's vent fluid does not primarily vent through the chimney and out like the other sites. Instead, the fluid is channelized through the flanges and up and over its cap, collecting in the center of the cap and creating several microenvironments of differing temperatures and chemistries (Teske *et al.,* 2016). These different habitats introduce a need for microbes to adapt quickly to an ever-changing environment which is supported by the enrichment of transposase genes and increased potential for horizontal gene transfer (He *et al.,* 2013).

Guaymas Basin is characterized by organic-rich sediment and high phytoplankton productivity supporting heterotrophic metabolisms (Teske *et al.,* 2002). These organic-rich sediments lead to a large amount of hydrocarbons to be used for energy via methanogenesis, like

is done in the hyperthermophilic class, Methanopyri (Dombrowski *et al.,* 2018). As expected, Methanopyri were abundant in Pagoda Chimney, further corroborating the presence of hydrocarbons. Microbes at Pagoda Chimney most commonly utilize the hydrocarbons present via the Wood-Ljundhal pathway, as methanogenesis is coupled with the Wood-Ljundhal pathway for carbon fixation in archaea (Hugler and Sievert, 2011). The low abundance of *coxAB* and *ccoNO* genes at Pagoda supports the idea that there is likely deoxygenation occurring inside the chimney (Teske *et al.,* 2016). This deoxygenation creates environments favorable for anaerobes such as *Methanopyri*.

However, Pagoda Chimney demonstrates the most diversity with regard to *rbcL* genes, with a higher presence of archaeal *rbcL* genes, likely due to the physical structure of the chimney allowing for many temperature and chemical gradients (Bohnke and Perner, 2019). It has been shown that RuBisCO can also be used for nucleotide salvage rather than carbon fixation in archaea, which could explain the high abundance of archaeal *rbcL* genes present (Wrighton *et al.,* 2016).

Sulfate reduction has been found to be common among microbial communities at Guaymas Basin hydrothermal chimneys. Microbes oxidize the plentiful hydrocarbons found at this site which in turn can be used as electron donors in sulfate reduction (He *et al.,* 2013). Both the oxidative and reductive versions of *dsrAB* were present in Pagoda. The only instance of archaeal *dsrAB* genes present were in the Archaeoglobi class, the only known archaeal class that is hyperthermophilic with a sulfate-reducing metabolism (Pillot *et al*., 2021).

Snap-Snap Chimney

Back arcs, like the Urashima Vent Field, can have a wide variation in pH, dissolved gases, and metal concentrations due to variation in magma chemistry (Trembath-Reichert *et al.,* 2019). The high abundance of chemotaxis proteins at Snap-Snap supports that reduced chemical

availability is on a steep gradient with organisms needing to have increased motility and sensors to locate a source. The presence of *napA*, periplasmic nitrate reductase is indicative of low oxygen presence and anaerobic respiration (Stewart *et al.,* 2002). The low oxygen concentration is evidenced at Snap-Snap by the large relative abundance of *ccoNO* cytochrome c oxidase genes. Another study on the Urashima Vent Field determined that the hydrothermal fluids from the vents at Urashima have a relatively low pH (Toki *et al.,* 2014).

Carbon fixation at Snap-Snap Chimney is likely occurring via all three pathways analyzed and is dominated by the rTCA cycle in Campylobacteria. Snap-Snap Chimney also has a high abundance of Gammaproteobacterial *rbcL* genes, consistent with previous analyses of the CBB cycle on the Mariana back-arc (Trembath-Reichert *et al.,* 2019). The presence of the *rbcL* gene mapped to *Deinococci*, an extremophile chemoorganotroph, and the high abundance of chemotaxis proteins could further indicate that the Snap-Snap Chimney is an extreme environment with variable chemical, temperature, and nutrient gradients.

Based on the relative abundances of dissimilatory nitrogen metabolism genes found at Snap-Snap Chimney, there likely is a large amount of nitrite to be used as an energy source. Snap-Snap's higher abundance of Proteobacterial *nirK* genes indicates a prevalence of denitrification. Ammonia-oxidizing archaea were not identified since all *amoA* genes were identified as Betaproteobacteria and Gammaproteobacteria, which is likely due to a low concentration of ammonium in the system (Li *et al.,* 2014). Despite the lack of ammonia-oxidizing archaea, previous analyses of archaeal denitrifiers have found that accumulation of organic material can increase *nirK* gene abundances, indicating that there may be organic material build-up at Snap-Snap Chimney as there are archaeal *nirK* genes present (Hou *et al.,* 2013).

Previous analyses of sulfur metabolism at hydrothermal vents showed that Aquificae were more abundant and active in less reducing fluids (low H_2S) and Campylobacteria in more reducing fluids (high H_2S) (Trembath-Reichert *et al.,* 2019). At Snap-Snap Chimney, there is a higher abundance of Campylobacteria, indicating a high prevalence of sulfate in the vent fluid (Zhou *et al.,* 2020). Deltaproteobacteria and Gammaproteobacteria have been found to have the ability to couple sulfate reduction with sulfur oxidation using the oxidative form of *dsrAB* (Muller *et al.,* 2015). Since these taxa both have both sulfur genes, coupled sulfur oxidation with sulfate reduction is likely occurring.

Snap-Snap Chimney at the Urashima Vent Field is characterized by having high concentrations of iron (Trembath-Reichert *et al.,* 2019), which is hypothesized to be due to low pH from magmatic volatiles on the Mariana back-arc (Toki *et al.,* 2014). Snap-Snap Chimney does have several taxa assigned to the *cyc2* gene; however, no Zetaproteobacterial cyc2 genes were identified in contrast to previous research (McAllister *et al.,* 2020). This could be because the Zetaproteobacterial *cyc2* ORFs are folded into the Gammaproteobacterial or unclassified bacterial category during annotation, as Zetaproteobacteria are a relatively new class (Emerson *et al.,* 2007).

Ultra-No-Chi-Chi Chimney

All three carbon fixation pathways are occurring at Ultra-No-Chi-Chi Chimney, with more genes assigned to rTCA and CBB cycles than the Wood Ljundhal pathway. Notably, Ultra-No-Chi-Chi has nearly the same number of *aclB* and *rbcL* genes, demonstrating that these pathways are both used for carbon fixation without one being necessarily favored over the other. The rTCA cycle is largely done by Campylobacteria, while the CBB cycle has a higher diversity of taxa. The highly relative abundance of both *ccoNO* and *coxAB* genes indicates that Ultra-No-Chi-Chi has a broad oxygen gradient, allowing for anaerobic and aerobic organisms to fix carbon.

Denitrification is the most prevalent form of nitrogen metabolism at Ultra-No-Chi-Chi Chimney, with more taxa at a higher abundance assigned to the *nirK* gene. Interestingly, *amoA* is completely absent from the Ultra-No-Chi-Chi Chimney while this gene was identified at Snap-Snap, its geographic neighbor.

At Ultra-No-Chi-Chi, there is a large relative abundance of both *dsrAB* and *soxAB* genes, which coupled with the high relative abundance of reductive archaeal *dsrAB* genes present in the Archaeoglobi class and unclassified Euryarchaeota highlights the significance of sulfur cycling at Ultra-No-Chi-Chi. The relatively higher abundance of Aquificae in this chimney demonstrates that oxygen is likely coupled to sulfur oxidation at Ultra-No-Chi-Chi, as Aquificae require oxygen to survive (Hou *et al.,* 2020).

Unexpectedly, Ultra-No-Chi-Chi has a lower abundance of iron receptor protein genes and there is also a lower abundance of *cyc2,* which could indicate that there is less iron present. This was unexpected, as other Urashima chimneys have been characterized as having high iron (McAllister *et al.,* 2020). Despite having no *cyc2* genes map to known iron oxidizer Zetaproteobacteria at Ultra-No-Chi-Chi, Zetaproteobacterial *nirK* and SSU genes were found. Previous analyses have demonstrated that iron oxidation is coupled with denitrification via *nirK* in Zetaproteobacteria (McAllister *et al.,* 2021). Therefore, the presence of Zetaproteobacterial *nirK* and SSU genes confirms their presence and therefore iron oxidation at this chimney despite no *cyc2* genes mapping to that class.

CONCLUSION

Metagenomic analysis of these five hydrothermal vent chimneys demonstrates how the chemical composition of the chimney impacts the microbes that reside there and their potential metabolisms. Each chimney hosts a unique collection of microorganisms with different

combinations of potential metabolic activities. Despite these distinctions, there were several uniting characteristics. Genes for DNA repair, chemotaxis, and transposases have been found to be at higher abundances at hydrothermal vent chimneys compared to other environmental microbial communities and could be a uniting identifier for these communities to adapt to the ever-changing chemical and physical conditions. The relative abundances of oxygen and carbon metabolism genes at each of the chimneys tell a distinct story of the availability of these compounds as energy sources in both active and inactive chimneys. High oxygen metabolism genes coupled with low carbon fixation genes could be used as a unique identifier for inactive chimneys, as shown with Ochre Chimney. The differences in carbon fixation genes and their metabolic plasticity demonstrate that chimney microbes can adapt to varying chemical compositions of the chimneys and that many of these metabolic pathways tend to be functionally redundant to thrive in a dynamic ecosystem.

Literature Cited

Andrews S. (2010). FastQC: a quality control tool for high throughput sequence data. http://www.bioinformatics.babraham.ac.uk/projects/fastqc

Ardyna, M., Lacour, L., Sergi, S., d'Ovidio, F., Sallee, J., Rembauville, M., Blain, S., Tagliabue, A., Schlitzer, R., Jeandel, C., Arrigo, K.R., Claustre, H. (2019). Hydrothermal vents trigger massive phytoplankton blooms in the Southern Ocean. *Nature Communications,* 10(2451). https://doi.org/10.1038/s41467-019-09973-6

Assié, A., Leisch, N., Meier, D.V., Gruber-Vodicka, H., Tegetmeyer, H.E., Meyerdierks, A., Kleiner, M., Hinzke, T., Joye, S., Saxton, M., Dubilier, N., Petersen, J.M. (2020). Horizontal acquisition of a patchwork Calvin cycle by symbiotic and free-living Campylobacterota (formerly Epsilonproteobacteria). *ISME J,* 14:104-122. https://doi.org/10.1038/s41396-019-0508-7

Beam, J., Jay, Z., Kozubal, M., Inskeep, W.P. (2014). Niche specialization of novel Thaumarchaeota to oxic and hypoxic acidic geothermal springs of Yellowstone National Park. *ISME J,* 8**:**938–951. https://doi.org/10.1038/ismej.2013.193

Bell, E., Lamminmäki, T., Alneberg, J., Andersson, A.F., Qian, C., Xiong, W., Hettich, R.L., Frutschi, M., Bernier-Latmani, R. (2020). Active sulfur cycling in the terrestrial deep subsurface. *ISME J,* 14(5):1260-1272. https://doi.org/10.1038/s41396-020-0602-x

Biggs, C.R., Yeager, L.A., Bolser, D.G., Bonsell, C., Dichiera, A.M., Hou, Z., Keyser, S.R., Khursigara, A.J., Lu, K., Muth, A.F., Negrete, B., Erisman, B.E. (2020). Does functional redundancy affect ecological stability and resilience? A review and meta-analysis. *Ecosphere,* 11(7). https://doi.org/10.1002/ecs2.3184

Böhnke, S., Perner, M. (2019). Seeking active RubisCOs from the currently uncultured microbial majority colonizing deep-sea hydrothermal vent environments. *ISME J* 13:2475-2488. https://doi.org/10.1038/s41396-019-0439-3

Bolger, A.M., Lohse, M., Usadel, B. (2014). Trimmomatic: a flexible trimmer for Illumina sequence data. *Bioinformatics*, 30(15):2114-2120. https://doi.org/10.1093/bioinformatics/btu170

Brazelton, W.J., Baross, J.A. (2009). Abundant transposases encoded by the metagenome of a hydrothermal chimney biofilm. *ISME J,* 3:1420-1424. https://doi.org/10.1038/ismej.2009.79

Buchfink, B., Xie, C., Huson, D.H. (2015). Fast and sensitive protein alignment using DIAMOND. *Nature Methods,* 12:59–60. https://doi.org/10.1038/nmeth.3176

Carini, P., Dupont, C.L., Santoro, A.E. (2018). Patterns of thaumarchaeal gene expression in culture and diverse marine environments. *Environmental Microbiology*, 20(6):2112–2124. https://doi.org/10.1111/1462-2920.14107

Chadwick, W.W., Paduan, J.B., Clague, D.A., Dreyer, B.M., Merle, S.G., Bobbitt, A.M., Caress, D.W., Philip, B.T., Kelley, D.S., Nooner, S.L. (2016). Voluminous eruption from a zoned magma body after an increase in supply rate at Axial Seamount. *Geophysical Research Letters,* 43(23):12063-12070. https://doi.org/10.1002/2016GL071327

Cuecas, A., Kanoksilapatham, W., Gonzalez, J.M. (2017). Evidence of horizontal gene transfer by transposase gene analyses in *Fervidobacterium* species. *PLoS ONE,* 12(4). https://doi.org/10.1371/journal.pone.0173961

de Gier, J.-W.L., Schepper, M., Reijnders, W.N.M., van Dyck, S.J., Slotboom, D.J., Warne, A., Saraste, M., Krab, K., Finel, M., Stouthamer, A.H., van Spanning, R.J.M. and van der Oost, J. (1996). Structural and functional analysis of aa_3-type and cbb_3-type cytochrome *c* oxidases of *Paracoccus denitrificans* reveals significant differences in proton-pump design. *Molecular Microbiology*, 20:1247-1260. https://doi.org/10.1111/j.1365-2958.1996.tb02644.x

Dick, G. J. (2019). The microbiomes of deep-sea hydrothermal vents: distributed globally, shaped locally. *Nature Reviews Microbiol*ogy, 17:271–283. https://doi.org/10.1038/s41579-019-0160-2

Dombrowski, N., Teske, A.P., Baker, B.J. (2018). Expansive microbial metabolic versatility and biodiversity in dynamic Guaymas Basin hydrothermal sediments. *Nature Communications,* 9(4999). https://doi.org/10.1038/s41467-018-07418-0

Edwards, K.J. (2004). Formation and degradation of seafloor hydrothermal sulfide deposits. "Sulfur Biogeochemistry - Past and Present", 379. https://doi.org/10.1130/0-8137-2379-5.83

Edwards, K.J., Rogers, D.R., Wirsen, C.O., McCollum, T.M. (2003). Isolation and Characterization of Novel Psychrophilic, neutrophilic, Fe-oxidizing, chemolithoautotrophic α- and γ-Proteobacteria from the Deep Sea. *Applied Environmental Microbiology,* 69(5):2906-2913. https://doi.org/10.1128/AEM.69.5.2906-2913.2003

Emerson, D., Rentz, J.A., Lilburn, T.G., Davis, R.E., Aldrich, H., Chan, C., Moyer, C.L. (2007). A Novel Lineage of Proteobacteria Involved in Formation of Marine Fe-Oxidizing Microbial Mat Communities. *PLoS one,* 2(8). https://doi.org/10.1371/journal.pone.0000667

Emerson, D., Moyer, C.L. (2015). Microbiology of Seamounts: Common Patterns Observed in Community Structure. *Oceanography,* 23(1):148-163. https://doi.org/10.5670/oceanog.2010.67

Fortin, D., Ferris, F.G., Scott, S.D. (1998). Fe-silicates and Fe-oxides on bacterial surfaces in samples collected near vents on the Southern Explorer Ridge in the northeast Pacific Ocean. *American Mineralogist,* 83(11-12):1399-1408. https://doi.org/10.2138/am-1998-11-1229

Fortunato, C.S., Larson, B., Butterfield, D.A., Huber, J.A. (2018). Spatially distinct, temporally stable microbial populations mediate biogeochemical cycling at and below the seafloor in hydrothermal vent fluids. *Environmental Microbiology,* 20(2):769-784. https://doi.org/10.1111/1462-2920.14011

Galambos, D., Anderson, R.E., Reveillaud, J. and Huber, J.A. (2019). Genome-resolved metagenomics and metatranscriptomics reveal niche differentiation in functionally redundant microbial communities at deep-sea hydrothermal vents. *Environmental Microbiology*, 21(11):4395-4410. https://doi.org/10.1111/1462-2920.14806

Garber, A.I., Nealson, K.H., Okamoto, A., McAllister, S.M., Chan, C.S., Barco, R.A., Merino, N. (2020). FeGenie: A comprehensive tool for the identification of iron genes and iron gene neighborhoods in genome and metagenome assemblies. *Frontiers in Microbiology* 11(37). https://doi.org/10.3389/fmicb.2020.00037

Han, Y., Gonnella, G., Adam, N., Schippers, A., Burkhardt, L., Kurtz, S., Schwarz-Schampera, U., Franke, H., Perner, M. (2018). Hydrothermal chimneys host habitat-specific microbial communities: analogues for studying the possible impact of mining seafloor massive sulfide deposits. *Nature Scientific Reports*, 8(10386). https://doi.org/10.1038/s41598-018-28613-5

He, Y., Feng, X., Fang, J., Zhang, Y., Xiao, X. (2015). Metagenome and metatranscriptome revealed a highly active and intensive sulfur cycle in an oil-immersed hydrothermal chimney in Guaymas Basin. *Frontiers in Microbiology,* 6(1236). https://doi.org/10.3389/fmicb.2015.01236

He, Y., Xiao, X., Wang, F. (2013). Metagenome reveals potential microbial degradation of hydrocarbon coupled with sulfate reduction in an oil-immersed chimney from Guaymas Basin. *Frontiers in Microbiology,* 4(148). https://doi.org/10.3389/fmicb.2013.00148

Hou, J., Cao, X., Song, C., Zhou, Y. (2013). Predominance of ammonia-oxidizing archaea and nirK-gene-bearing denitrifiers among ammonia-oxidizing and denitrifying populations in sediments of a large ubran eutrophic lake (Lake Donghu). *Canadian Journal of Microbiology*, *59*(7):456–464. https://doi.org/10.1139/cjm-2013-0083

Hou, J., Sievert, S.M., Wang, Y., Seewald, J.S., Natarajan, V.P., Wang, F., Xiao, X. (2020). Microbial succession during the transition from active to inactive stages of deep-sea hydrothermal vent sulfide chimneys. *Microbiome,* 8(102). https://doi.org/10.1186/s40168-020-00851-8

Hugler, M., Sievert, S.M. (2011). Beyond the Calvin Cycle: Autotrophic Carbon Fixation in the Ocean. *Annual Review of Marine Science,* 3:261-289. https://doi.org/10.1146/annurev-marine-120709-142712

Hyatt, D., Chen, G.L., LoCascio, P.F., Land, M.L., Larimer, F.W., Hauser, L.J. (2010). Prodigal: prokaryotic gene recognition and translation initiation site identification. *BMC Bioinformatics,* 11(119). https://doi.org/10.1186/1471-2105-11-119

Jesser, K.J., Fullerton, H., Hager, K.W., Moyer, C.L. (2015). Quantitative PCR analysis of functional genes in iron-rich microbial mats at an active hydrothermal vent system (Lō'ihi Seamount, Hawai'i). *Applied and environmental microbiology*, 81(9):2976–2984. https://doi.org/10.1128/AEM.03608-14

Kang, D.D., Froula, J., Egan, R., and Wang, Z. (2015). MetaBAT, an efficient tool for accurately reconstructing single genomes from complex microbial communities. *PeerJ*, 3:e1165. https://doi.org/10.7717/peerj.1165

Kato, S. Shibuya, T., Takaki, Y., Hirai, M., Nunoura, T., Suzuki, K. (2018). Genome-enabled metabolic reconstruction of dominant chemosynthetic colonizers in deep-sea massive sulfide deposits. *Environmental Microbiology*, 20(2):862-877. https://doi.org/10.1111/1462-2920.14032

Kerou, M., Offre, P., Valledor, L., Schleper, C. (2016). Proteomic and comparative genomics of *Nitrososphaeria viennensis* reveal the core genome and adaptations of archaeal ammonia oxidizers. *PNAS,* 113(49). https://doi.org/10.1073/pnas.1601212113

Langmead B., Salzberg S. (2012). Fast gapped-read alignment with Bowtie 2. *Nature Methods,* 9(4):357-359. https://doi.org/10.1038/nmeth.1923

Li, D., Liu, C., Luo, R., Sadakane, K., Lam, T. (2015). MEGAHIT: an ultra-fast single-node solution for large and complex metagenomics assembly via succinct *de Bruijn* graph, *Bioinformatics,* 31(10):1674-1676. https://doi.org/10.1093/bioinformatics/btv033

Li, J., Nedwell, D.B., Beddow, J., Dumbrell, A.J., McKew, B.A., Thorpe, E.L., Whitby, C. (2014). *amoA* gene abundances and nitrification potential rates suggest that benthic ammonia-oxidizing bacteria and not archaea dominate N cycling in the Colne Estuary, United Kingdom. *Applied and Environmental Microbiology,* 81(1). https://doi.org/10.1128/AEM.02654-14

Mattes, T.E., Nunn, B.L., Marshall, K.T., Proskurowski, G., Kelley, D.S., Kawka, O.E., Goodlett, D.R., Hansell, D.A., Morris, R.M. (2013). Sulfur oxidizers dominate carbon fixation at a biogeochemical hot spot in the dark ocean. *ISME J,* 7:2349–2360. https://doi.org/10.1038/ismej.2013.113

McAllister, S.M., Polson, S.W., Butterfield, D.A., Glazer, B.T., Sylvan, J.B., Chan, C.S. (2020). Validating the Cyc2 neutrophilic iron oxidation pathway using meta-omics of *Zetaproteobacteria* iron mats and marine hydrothermal vents. *American Society for Microbiology,* 5(1). https://doi.org/10.1128/mSystems.00553-19

McAllister, S.M., Vandzura, R., Keffer, J.L., Polson, S.W., Chan, C.S. (2021). Aerobic and anaerobic iron oxidizers together drive denitrification and carbon cycling at marine iron-rich hydrothermal vents. *ISME,* 15:1271-1286. https://doi.org/10.1038/s41396-020-00849-y

Meier D.V., Pjevac, P., Bach, W., Markert, S., Schweder, T., Jamieson, J. Petersen, S., Amann, R., Meyerdierks, A. (2019). Microbial metal-sulfide oxidation in inactive hydrothermal vent chimneys suggested by metagenomic and metaproteomic analyses. *Environmental Microbiology,* 21(2):682-701. https://doi.org/10.1111/1462-2920.14514

Meyer-Dombard, D.R., Amend, J.P., Osburn, M.R. (2012). Microbial diversity and potential for arsenic and iron biogeochemical cycling at an arsenic-rich, shallow-sea hydrothermal vent (Tutum Bay, Papua New Guinea). *Chemical Geology,* 348:37-47. https://doi.org/10.1016/j.chemgeo.2012.02.024

Mikheenko, A., Saveliev, V., Gurevich, A. (2016). MetaQUAST: evaluation of metagenome assemblies. *Bioinformatics*, 32(7):1088–1090. https://doi.org/10.1093/bioinformatics/btv697

Mori, J.F., Scott, J.J., Hager, K.W., Moyer, C.L., Kusel, K., Emerson, D. (2017). Physiological and ecological implications of an iron- or hydrogen-oxidizing member of the Zetaproteobacteria, *Ghiorsea bivora*, gen. nov., sp. nov.. *ISME J,* 11:2624–2636. https://doi.org/10.1038/ismej.2017.132

Muller, A.L., Kjeldsen, K.U., Rattei, T., Pester, M., Loy, A. (2015). Phylogenetic and environmental diversity of DSRAB-type dissimilatory (bi)sulfite reductases. *ISME J,* 9(5):1152-1165. https://doi.org/10.5670/oceanog.2010.67

O'Brien, C.E., Giovannelli, D., Govenar, B., Luther, G.W., Lutz, R.A., Shank, T.M., Vetriani, C. (2015). Microbial biofilms associated with fluid chemistry and megafaunal colonization at post-eruptive deep-sea hydrothermal vents. *Deep. Res. Part II Top. Stud. Oceanogr.* 121:31-40. https://doi.org/10.1016/j.dsr2.2015.07.020

Oksanen, J., Kindt, R., Legendre, P., O'Hara, B., Simpson, G., Solymos, P., Stevens, M., Wagner, H. (2008). Vegan: Community Ecology Package. *R package version 1.15-1.*

Opatkiewicz, A.D., Butterfield, D.A., Baross, J.A. (2009). Individual hydrothermal vents at Axial Seamount harbor distinct subseafloor microbial communities. *FEMS Microbial Ecology,* 70:413-424. https://doi.org/10.1111/j.1574-6941.2009.00747.x

Oren, A., Garrity, G.M. (2021). Valid publication of the names of forty-two phyla of prokaryotes. *International Journal of Systematic and Evolutionary Microbiology,* 71(10). https://doi.org/10.1099/ijsem.0.005056

Orcutt, B.N., Bradley, J.A., Brazelton, W.J., Estes, E.R., Goordial, J.M., Huber, J.A., Jones, R.M., Mahmoud, N., Marlow, J.J. Murdock, S., Pachiadaki, M. (2020). Impacts of deep-sea mining on microbial ecosystem services. *Limnology and Oceanography,* 65:1489-1510. https://doi.org/10.1002/lno.11403

Oulas A., Polymenakou P.N., Seshadri R., Tripp H.J., Mandalakis M., Paez-Espino A.D., Pati, A., Chain, P., Nomikou, P., Carey, S., Kilias, S., Christakis, C., Kotoulas, G., Magoulas, A., Ivanova, N.N., Kyrpides, N.C. (2016). Metagenomic investigation of the geologically unique Hellenic volcanic arc reveals a distinctive ecosystem with unexpected physiology. *Environmental Microbiology,* 18:1122–1136. https://doi.org/10.1111/1462-2920.13095

Pan, J., Xu, W., Zhou, Z., Shao, Z., Dong, C., Liu, L., Luo, Z., Li, M. (2022). Genome-resolved evidence for functionally redundant communities and novel nitrogen fixers in the deyin-1 hydrothermal field, Mid-Atlantic Ridge. *Microbiome,* 10(8). https://doi.org/10.1186/s40168-021-01202-x

Parks, D.H., Imelfort, M., Skennerton, C.T., Hugenholtz, P., Tyson, G.W. (2015). CheckM: assessing the quality of microbial genomes recovered from isolates, single cells, and metagenomes. *Genome research*, *25*(7):1043–1055. https://doi.org/10.1101/gr.186072.114

Pillot, G., Ali, O.A., Davidson, S., Shintu, L., Godfroy, A., Combet-Blanc, Y., Bonin, P., Liebgott, P. (2021). Identification of enriched hyperthermophilic microbial communities from a deep-sea hydrothermal vent chimney under electrolithoautotrophic culture conditions. *Nature Scientific Reports,* 11(14782). https://doi.org/10.1038/s41598-021-94135-2

Puente-Sánchez, F., García-García, N., Tamames, J. (2020). SQMtools: automated processing and visual analysis of 'omics data with R and anvi'o. *BMC Bioinformatics,* 21**(**358). https://doi.org/10.1186/s12859-020-03703-2

Ragsdale, S.W., Pierce, E. (2008). Acetogenesis and the Wood-Ljungdahl pathway of CO(2) fixation. *Biochimica et biophysica acta*, 1784(12):1873–1898. https://doi.org/10.1016/j.bbapap.2008.08.012

Reznikoff, W.S. (2003). Tn5 as a model for understanding DNA transposition. *Molecular Microbiology,* 47(5):1199-2016. https://doi.org/10.1046/j.1365-2958.2003.03382.x

Seemann, T. (2014). Prokka: rapid prokaryotic genome annotation. *Bioinformatics,* 30(14): 2068-2069. https://doi.org/10.1093/bioinformatics/btu15

Sieber, C.M.K., Probst, A.J., Sharrar, A., Thomas, B.C., Hess, M., Tringe, S.G., Banfield, J.F. (2018). Recovery of genomes from metagenomes via a dereplication, aggregation and scoring strategy. *Nature Microbiology,* 3:836–843. https://doi.org/10.1038/s41564-018-0171-1

Stewart, V., Lu, Y., Darwin, A.J. (2002). Periplasmic Nitrate Reductase (NapABC Enzyme) Supports Anaerobic Respiration by *Escherichia coli* K-12. *Journal of Bacteriology,* 184(5):1314–1323. https://doi.org/10.1128/JB.184.5.1314-1323.2002

Sylvan, J.B., Toner, B.M., Edwards, K.J. (2012). Life and death of deep-sea vents: bacterial diversity and ecosystem succession on inactive hydrothermal sulfides. *MBio,* 3(1). https://doi.org/10.1128/mBio.00279-11

Sylvan, J.B., Wankel, S.D., LaRowe, D.E., Charoenpong, C.N., Huber, J.A., Moyer, C.L., Edwards, K.J. (2017). Evidence for microbial mediation of subseafloor nitrogen redox processes at Loihi Seamount, Hawaii. *Geochimica et Cosmochimica Acta*, 198:131-150. https://doi.org/10.1016/j.gca.2016.10.029

Tamames, J., Puente-Sanchez, F. (2019). SqueezeMeta, a highly portable, fully automatic, metagenomics pipeline. *Frontiers in Microbiology,* 9(3394). https://doi.org/10.3389/fmicb.2018.03349

Teske, A., de Beer, D., McKay, L.J., Tivey, M.K., Biddle, J.F., Hoer, D., Lloyd, K.G., Lever, M.A., Røy, H., Albert, D.B., Mendlovitz, H.P., MacGregor, B.J. (2016). The Guaymas Basin Hiking Guide to Hydrothermal Mounds, Chimneys, and Microbial Mats: Complex Seafloor Expressions of Subsurface Hydrothermal Circulation. *Frontiers in Microbiology,* 7(75). https://doi.org/10.3389/fmicb.2016.00075

Teske, A., Hinrichs, K., Edgcomb, V., de Vera Gomez, A., Kysela, D., Sylva, S.P. Sogin, M.L., Jannasch, H.W. (2002). Microbial diversity of hydrothermal sediments in the Guaymas Basin: Evidence for anaerobic methanotrophic communities. *Applied and Enviornmental Microbiology,* 68(4). https://doi.org/10.1128/AEM.68.4.1994-2007.2002

Toki, T. Ishibashi, J., Noguchi, T., Tawata, M., Tsunogai, U., Yamanaka, T., Nakamura, K. (2014). Chemical and isotopic compositions of hydrothermal fluids at Snail, Archaean, Pika, and Urashima sites in the Southern Mariana Trough. *Subseafloor Biosphere Linked to Hydrothermal Systems. Springer, Tokyo*: 587-602. https://doi.org/10.1007/978-4-431-54865-2_45

Trembath-Reichert, E., Butterfield, D.A., Huber, J.A. (2018). Active subseafloor microbial communities from Mariana back-arc venting fluids share metabolic strategies across different thermal niches and taxa. *ISME,* 13:2264-2279. https://doi.org/10.1038/s41396-019-0431-y

Tunnicliffe, V., Botros, M., de Burgh, M.E., Dinet, A., Johnson, H.P., Juniper, S.K., McDuff, R.E. (1985). Hydrothermal vents of Explorer Ridge, northeast Pacific. *Deep-Sea Research,* 33(3):401-412. https://doi.org/10.1016/0198-0149(86)90100-7

Waite, D.W., Vanwonterghem, I., Rinke, C., Parks, D.H., Zhang, Y., Takai, K., Sievert, S.M., Simon, J., Campbell, B.J., Hanson, T.E., Woyke, T., Klotz, M.G. and Hugenholtz, P. (2017). Comparative Genomic Analysis of the Class *Epsilonproteobacteria* and Proposed Reclassification to Epsilonbacteraeota (phyl. nov.). *Frontiers in Microbiology*, 8:682. https://doi.org/10.3389/fmicb.2017.00682

Wang, Q., Garrity, G.M., Tiedje, J.M., Cole, J.R. (2007). Naïve Bayesian classifier for rapid assignment of rRNA sequences into the new bacterial taxonomy. *Applied Environmental Microbiology,* 73:5261–5267. https://doi.org/10.1128/AEM.00062-07

Wickham, H. (2016). *ggplot2: Elegant Graphics for Data Analysis*. Springer-Verlag New York. ISBN 978-3-319-24277-4, https://ggplot2.tidyverse.org

Wright, J.P., Jones, C.G., Flecker, A.S. (2002) An ecosystem engineer, the beaver, increases species richness at the landscape scale. *Oecologia,* 132:96–101. https://doi.org/10.1007/s00442-002-0929-1

Wrighton, K.C., Castelle, C.J., Varaljay, V.A., Satagopan, S., Brown, C.T., Wilkins, M.J., Thomas, B.C., Sharon, I., Williams, K.H., Tabita, F.R., Banfield, J.F. (2016). RubisCO of a nucleoside pathway known from Archaea is found in diverse uncultivated phyla in bacteria. *ISME J,* 10:2702–2714. https://doi.org/10.1038/ismej.2016.53

Wu, Y.W., Simmons, B.A., Singer, S.W. (2015). MaxBin 2.0: an automated binning algorithm to recover genomes from multiple metagenomic datasets. *Bioinformatics,* 32(4):605–607. https://doi.org/10.1093/bioinformatics/btv638

Xie, W., Wang, F., Guo, L. Chen, Z., Sievert, S.M., Meng, J., Huang, G., Li, Y., Yan, Q., Wu, S., Wang X., Chen S., He, G., Xiao, X., Xu, A. (2011). Comparative metagenomics of microbial communities inhabiting deep-sea hydrothermal vent chimneys with contrasting chemistries. *ISME J,* 5**:**414–426. https://doi.org/10.1038/ismej.2010.144

Zhou, G., Yin, J., Chen, H., Hua, Y., Sun, L., Gao, H. (2013). Combined effect of loss of the caa3 oxidase and Crp regulation drives Shewanella to thrive in redox-stratified environments. *ISME J*, *7*(9):1752–1763. https://doi.org/10.1038/ismej.2013.62

Zhou, Z., St. John, E., Anantharaman, K., Reysenbach, A-L. (2022). Global patterns of diversity and metabolism of microbial communities in deep-sea hydrothermal vent deposits. *Microbiome,* 10(241). https://doi.org/10.1186/s40168-022-01424-7

Table 1. A summary of samples collected from five different hydrothermal vent chimneys. Chemistry data for Axial Castle Chimney is taken from Butterfield, *et al.,* 1990.

Chimney Sample	**Dive Number**	**Collection DSV**	**Date**	**Latitude & Longitude**	**Depth (m)**	**Temp (°C)**	**Fe (µM)**	**H_2S (µM)**	**H_2 (µM)**
Magic Mountain: Ochre	R668	ROV ROPOS	07/29/2002	49°45.38'N, 130°15.75'W	1847	4	NA	NA	NA
Axial: Castle	R674	ROV ROPOS	08/04/2002	45°55.57'N, 129°58.80'W	1522	235	31	7.1	1.5
Guaymas: Pagoda	A2838	HOV ALVIN	10/07/1994	27°00.91'N, 111°24.64'W	1980	279	NA	NA	NA
Urashima: Snap-Snap	J2-797	ROV JASON II	11/01/2014	12°55.33'N, 143°38.95'W	2928	161	48.5	<0.4	0.01
Urashima: Ultra-No-Chi-Chi	J2-801	ROV JASON II	12/18/2014	12°55.34'N, 143°38.95'W	2929	174	48.5	<0.4	0.01

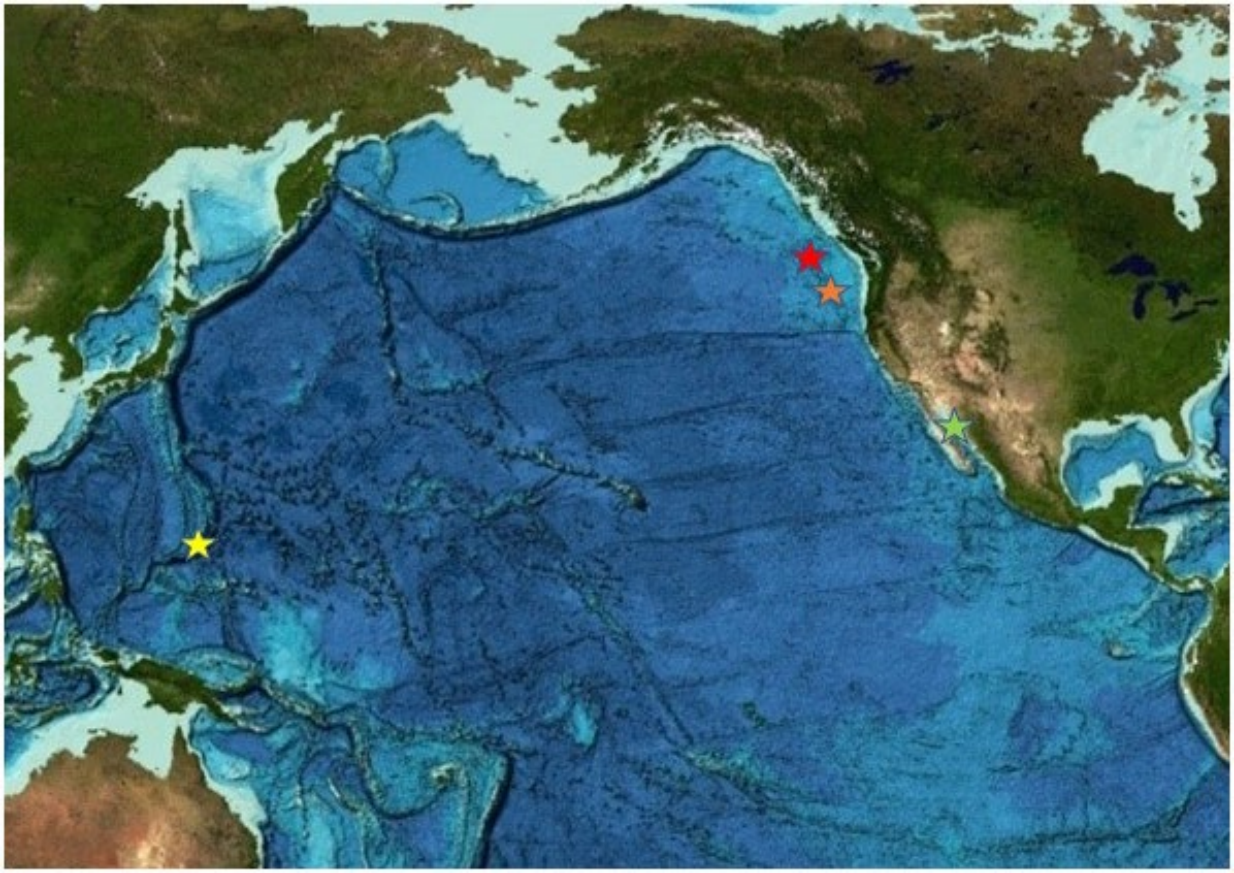

Figure 1. Map of the four sampling locations across the Pacific Ocean. The red star denotes the Magic Mountain, Explorer Ridge sampling location of the Ochre Chimney, the orange star denotes the Axial Volcano, Juan de Fuca Ridge sampling location of the Castle Chimney. The green star denotes the Guaymas Basin sampling location of the Pagoda Chimney. The yellow star denotes the Mariana back-arc Urashima sampling location of the Snap-Snap and Ultra-No-Chi-Chi Chimneys. (Image reproduced from the GEBCO world map 2019, www.gebco.net.)

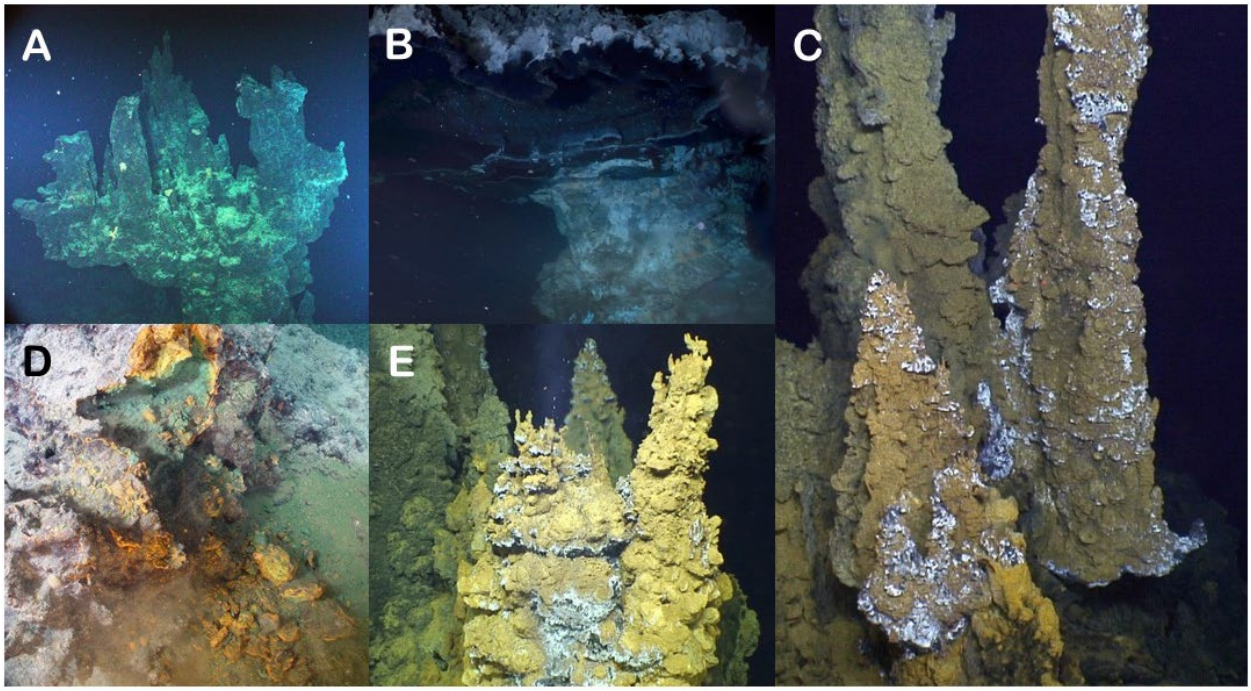

Figure 2. Photos of the five chimneys evaluated in this study. (A) Castle Chimney from Axial Seamount. (B) Pagoda Chimney from Guaymas Basin. (C) Ultra-No-Chi-Chi Chimney from the Urashima Vent Field (Laser dots are 10 cm apart). (D) Ochre Chimney from Magic Mountain. (E) Snap-Snap Chimney also from the Urashima Vent Field.

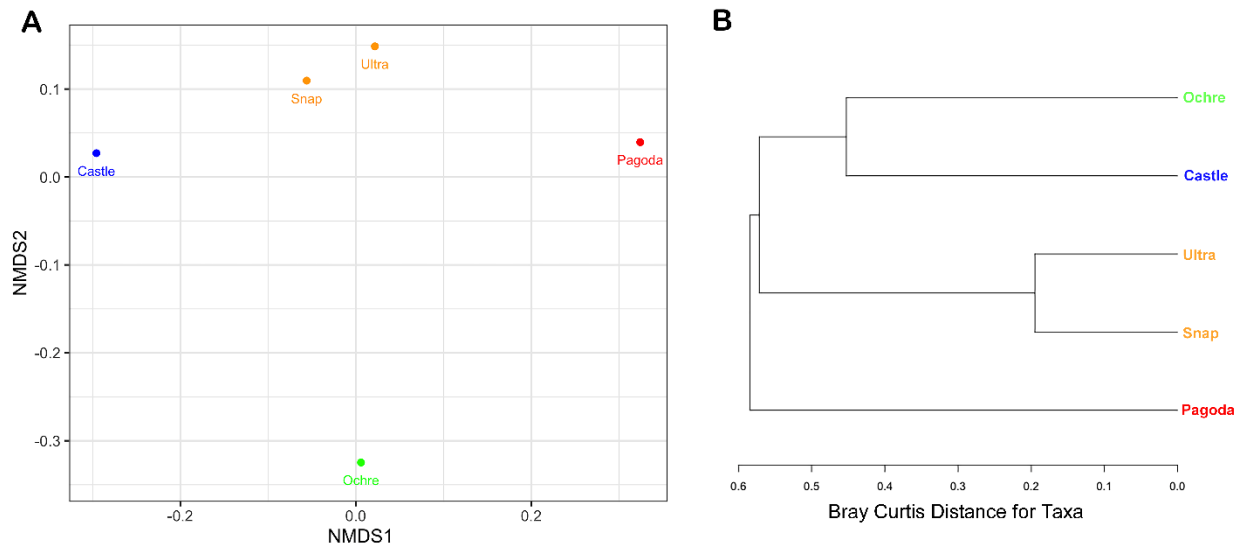

Figure 3. (A) NMDS plot using Bray-Curtis distance metric with the chimneys labeled with colored dots by location. The blue dot represents Castle Chimney at Axial Seamount, green represents Ochre Chimney at Magic Mountain, red represents Pagoda Chimney at Guaymas Basin Vent Field and orange represents the Snap-Snap and Ultra-No-Chi-Chi Chimneys from the Urashima Vent Field. (B) Cluster dendrogram of taxa similarities among chimneys. Bray Curtis distance metric was used to cluster each chimney based on differences in taxa composition.

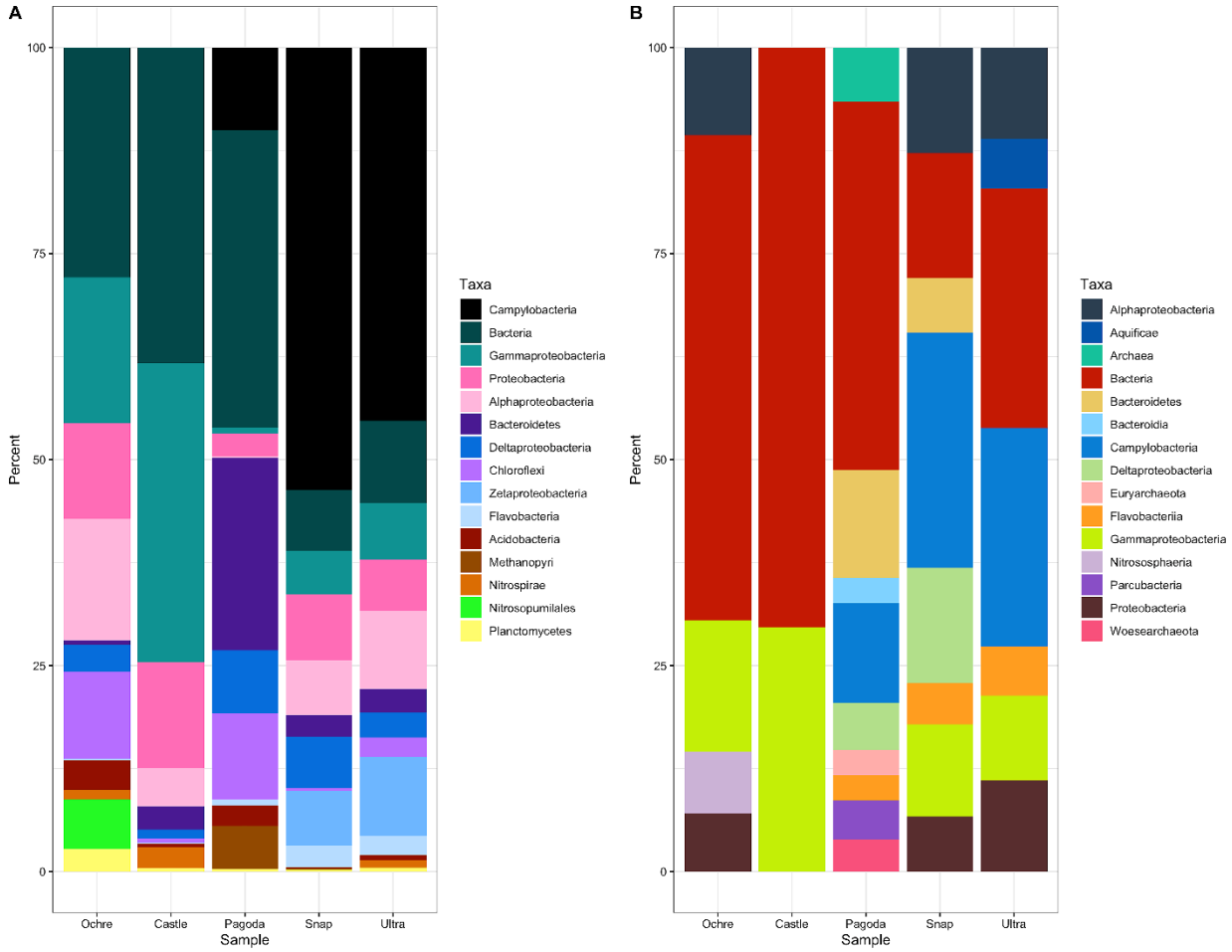

Figure 4. Stacked bar graph of the top 15 microbial taxa found in each chimney as a percentage of reads from the whole metagenome. (A) Stacked bar graph of the ORFs from assembly, not including unclassified or unmapped reads. (B) Stacked bar graph of the SSU rRNA gene reads, only including the top 15 taxa, not including unclassified or unmapped reads.

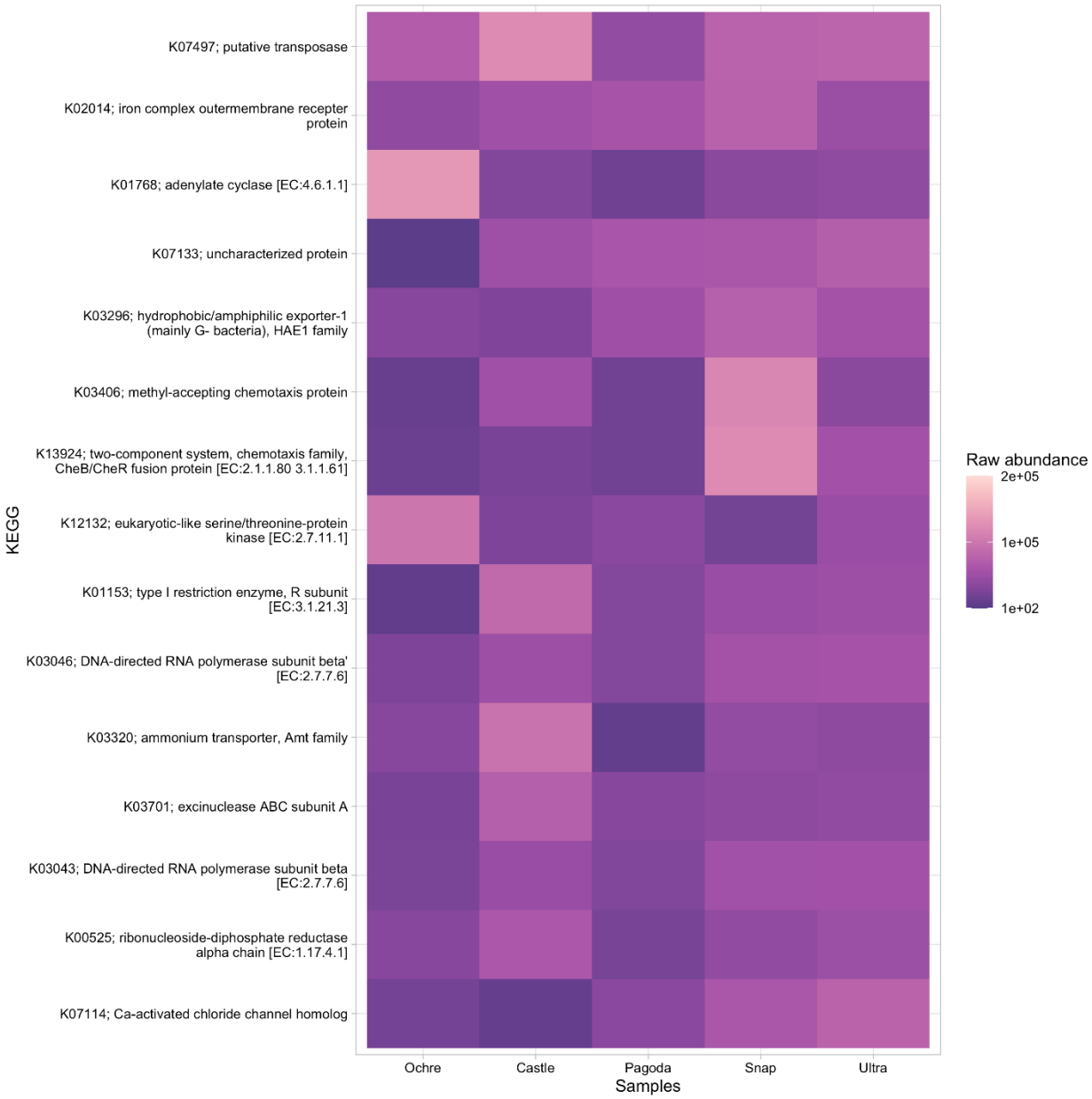

Figure 5. Heatmap of the top 15 most abundant KEGG genes found in all five chimneys. Presence is measured in raw abundance of reads.

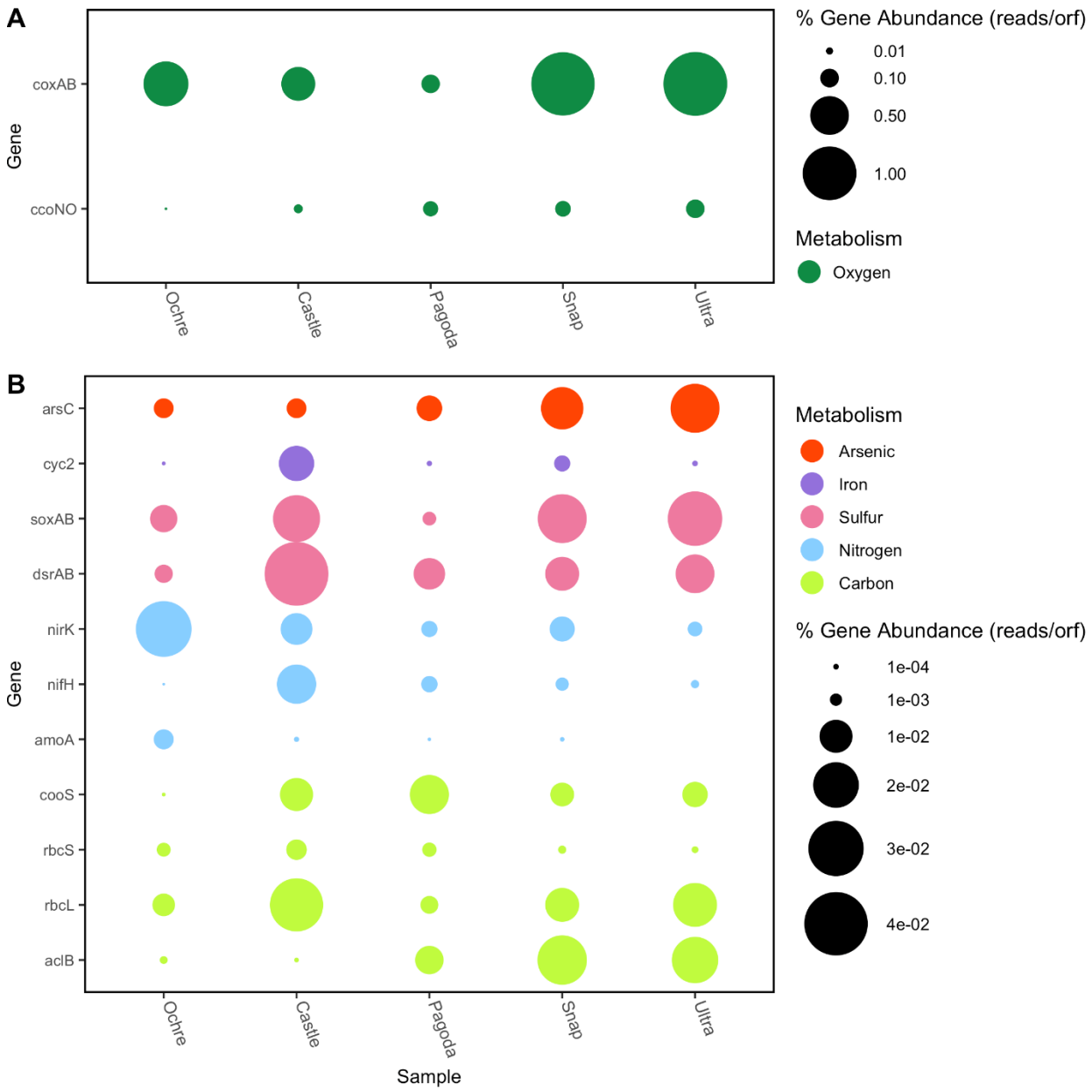

Figure 6. Bubble plot of the relative abundance of key metabolic genes found in each chimney. Relative abundance is measured in the number of reads per ORF divided by total number of reads. (A) Oxygen metabolism genes represented by dark green bubbles. (B) Arsenic, Iron, Sulfur, Nitrogen and Carbon genes. Red bubbles represent arsenic cycling genes, purple bubbles represent iron cycling genes, pink bubbles represent sulfur cycling genes, blue bubbles represent nitrogen cycling genes, and lime green bubbles represent carbon cycling genes.

Supplemental Table 1. MAGs and their taxonomic assignments with completeness and contamination.

Bin	Taxa	Length	GC %	Number of Contigs	Disparity	Completeness	Contamination	Strain Heterogeneity
metabat2.48	Proteobacteria	1298003	56.2	248	0	52.49	0.84	100
metabat2.10	Deltaproteobacteria	1464749	47.93	255	0.032	50.1	0.8	0
metabat2.24	Bacteroidetes	2002372	45.87	404	0.036	43.27	0	0
metabat2.38	Actinobacteria	821088	64.03	239	0	41.31	4.76	50
metabat2.42	Bacteria	443507	40.84	77	0	41.14	3.61	0
metabat2.15	Calditrichaeota	782889	46.05	175	0.182	37.46	0	0
metabat2.63	Gemmatimonadetes	795028	62.62	180	0.124	34.56	0	0
metabat2.22	Deltaproteobacteria	1157082	47.48	63	0	34.19	0.07	0
metabat2.46	Spirochaetes	1267710	56.92	194	0.062	33.52	1.57	0
metabat2.40	Bacteria	543747	50.47	51	0	32.13	1.72	0
metabat2.2	Campylobacteria	688607	32.15	153	0.18	29.53	1.88	15.38
metabat2.26	Bacteria	1138543	50.56	133	0	27.74	1.72	0
metabat2.43	Bacteria	353357	37.65	72	0	26.8	1.88	0
metabat2.28	Bacteria	845593	50.56	179	0	26.02	0	0
metabat2.44	Bacteria	664143	46.57	85	0	24.14	0	0
metabat2.34	Actinobacteria	575531	69.38	168	0.037	22.91	0	0
metabat2.23	Bacteroidetes	432648	38.3	69	0	20.51	0	0
metabat2.45	Gemmatimonadetes	508301	49.59	80	0	18.97	0	0
metabat2.55	Deltaproteobacteria	573947	50.01	30	0	18.21	0	0
metabat2.56	Deltaproteobacteria	420040	47.14	70	0	17	0	0

metabat2.21	Bacteroidia	562460	41.13	128	0.099	16.89	0	0
metabat2.62	Gammaproteobacteria	441353	44.93	88	0	16.45	0.21	0
metabat2.27	Bacteroidetes	367914	39.52	44	0	16.41	0	0
metabat2.11	Campylobacteria	345372	34.05	97	0.152	16.24	0.2	40
metabat2.13	Bacteroidetes	582376	45.96	66	0	16.15	0	0
metabat2.17	Bacteroidetes	581793	39.05	76	0	16.07	0	0
metabat2.6	Flavobacteriia	444509	28.99	136	0.022	15.65	0.65	50
metabat2.20	Bacteria	482624	47.68	41	0	15.52	0	0
metabat2.54	Campylobacteria	355921	33.72	102	0.061	15.29	0.28	33.33
metabat2.51	Campylobacteria	277457	30.77	76	0	14.65	0	0
metabat2.58	Thermoplasmata	249099	44.04	25	0	14.21	0.28	0
metabat2.47	Campylobacteria	359569	30.37	112	0	13.93	1.28	0
metabat2.39	Calditrichaeota	588168	47.43	115	0.259	13.79	0	0
metabat2.32	Zetaproteobacteria	315076	52.37	56	0.049	13.22	0.09	0
metabat2.3	Gammaproteobacteria	290448	57.08	80	0	12.97	0	0
metabat2.33	Candidatus Gracilibacteria	232636	21.77	55	0.125	12.07	0	0
metabat2.16	Bacteria	220201	39.39	11	0	12.07	0	0
metabat2.36	Candidatus Cloacimonetes	205900	38.95	57	0.443	12.07	0	0
metabat2.60	Campylobacteria	307591	33.39	53	0.156	11.57	0.41	0
metabat2.61	Nitrospirae	243267	59.55	58	0.107	11.19	0	0
metabat2.31	Candidatus Gracilibacteria	242523	23.3	45	0.148	10.92	0.86	100
metabat2.41	Candidatus Bipolaricaulota	225858	66.05	41	0	10.85	0	0
metabat2.49	Nitrospinia	269898	53.43	55	0	10.34	0	0

metabat2.9	Bacteroidetes	224133	40.24	28	0	9.74	0.51	100
metabat2.29	Bacteroidetes	264380	44.2	39	0	9.56	0	0
metabat2.52	Bacteroidia	322320	40.13	83	0	9.27	0	0
metabat2.57	Campylobacteria	235128	32.98	49	0	9.23	0	0
metabat2.35	Betaproteobacteria	200733	44.25	34	0	9.22	0	0
metabat2.12	Candidatus Fermentibacteria	295485	49.17	55	0	8.62	0	0
metabat2.7	Alphaproteobacteria	288804	56.93	61	0	8.5	0	0
metabat2.19	Flavobacteriia	247701	30.52	67	0	8.2	0	0
metabat2.18	Bacteroidetes	211544	51.81	37	0	7.69	0	0
metabat2.8	Acidobacteria	297429	70.72	70	0.042	7.61	0	0
metabat2.64	Alphaproteobacteria	286760	54.95	60	0	7.43	0	0
metabat2.30	Gammaproteobacteria	258601	46.27	46	0.133	7.3	0	0
metabat2.1	Deltaproteobacteria	207298	45.56	27	0	7.2	0	0
metabat2.25	Bacteria	373313	48.42	87	0	6.11	0	0
metabat2.50	Deltaproteobacteria	606366	70.97	155	0.026	6	0	0
metabat2.5	Gammaproteobacteria	200928	48.79	44	0	5.39	0	0
metabat2.14	Bacteria	216750	47.92	24	0	5.17	0	0
metabat2.4	Campylobacteria	210151	34.45	34	0.305	4.93	0.16	0
metabat2.37	Acidimicrobiia	227805	62.45	53	0.233	2.52	0	0
metabat2.53	Gemmatimonadetes	217649	63.37	50	0.199	0	0	0

Supplemental Table 2. Relative abundance of different autotrophy genes and their taxonomic assignment for Ochre Chimney.

Taxa	*rbcS* (%)	*rbcL* (%)	*aclB* (%)	*cooS* (%)	*amoA* (%)	*nifH* (%)	*nirK* (%)	*dsrAB* (%)	*soxAB* (%)	*cyc2* (%)	*arsC* (%)	*ccoNO* (%)	*coxAB* (%)
Acidimicrobiia							4.72E-05						4.27E-03
Acidobacteria		3.22E-05					1.89E-04				4.29E-06		1.64E-02
Acidobacteriia													7.70E-05
Actinobacteria							1.07E-04				4.51E-05		1.50E-02
Actinomycetia		8.59E-06					2.58E-05				4.29E-06		1.73E-03
Alphaproteobacteria		2.06E-04				2.15E-06	9.45E-04	5.15E-05	2.77E-03	1.72E-05	1.27E-04		1.17E-01
Anaerolineae							3.65E-04						8.66E-04
Archaea		1.29E-05			7.24E-04		4.55E-03						2.19E-02
Ardenticatenia													3.85E-05
Bacilli											2.15E-06		
Bacteria	1.37E-03		4.29E-06	1.07E-05	2.15E-06		4.08E-03	6.66E-05	5.15E-05		2.23E-04	2.50E-04	9.21E-02
Bacteroidetes							1.07E-04			6.29E-04	8.59E-06	3.85E-05	1.62E-03
Betaproteobacteria		3.33E-04			2.88E-04		4.21E-04		1.72E-05		4.51E-05		1.10E-02
Calditrichae													6.73E-04
Calditrichaeota													1.35E-04
Campylobacteria			4.29E-06										1.92E-05
Candidatus Bipolaricaulota													3.85E-05
Candidatus Dadabacteria							1.07E-05				4.29E-06		1.54E-04
Candidatus Eisenbacteria													3.85E-05
Candidatus Omnitrophica							1.29E-05				1.29E-05		4.43E-04
Candidatus Peregrinibacteria													3.85E-05
Candidatus Tectomicrobia													1.35E-04
Chitinophagia													3.08E-04
Chlorobi												3.85E-05	
Chloroflexi		2.15E-05					3.80E-04				3.86E-05	1.15E-04	6.15E-02

Crenarchaeota							4.29E-06						
Cyanobacteria		2.00E-04											
Cytophagia							4.29E-06					1.35E-04	2.69E-04
Dehalococcoidia													9.62E-04
Deinococci													3.85E-05
Deltaproteobacteria		3.44E-05		4.29E-06	8.59E-06		2.15E-04	4.29E-06		4.66E-05	3.01E-05	7.70E-05	1.71E-02
Elusimicrobia							4.29E-06						2.31E-04
Flavobacteriia							9.02E-05					1.92E-04	2.12E-04
Gammaproteobacteria		4.72E-04			1.50E-05		9.45E-04	1.72E-03	2.25E-03	1.04E-02	1.86E-03		1.19E-01
Gemmatimonadetes		1.22E-04					3.56E-04				7.51E-05	9.04E-04	2.88E-02
Ignavibacteria											4.29E-06		1.10E-03
Nitrososphaeria					7.06E-04		1.08E-02				6.44E-05		5.37E-02
Nitrospinae							1.37E-04		1.29E-05		1.10E-04		1.58E-03
Nitrospinia							1.85E-04				5.37E-05	7.70E-05	7.70E-05
Nitrospira			3.44E-05				4.29E-05						6.93E-04
Nitrospirae		1.29E-05	2.45E-04				1.57E-04				9.45E-05		9.24E-04
Oligoflexia													3.85E-05
Opitutae													1.15E-04
Phycisphaerae													9.24E-04
Planctomycetes							1.07E-05					1.35E-04	6.52E-03
Planctomycetia											4.29E-06	1.92E-05	1.31E-03
Proteobacteria		2.68E-03			8.59E-06		2.87E-03	7.88E-04	1.48E-03		3.78E-04	2.12E-04	6.67E-02
Rhodothermae		5.37E-05					3.22E-05						
Saprospiria													3.85E-05
Spirochaetia													3.85E-05
Thaumarchaeota		1.07E-04			1.47E-03		3.31E-03						3.84E-02
Verrucomicrobia							8.59E-06						3.46E-04
Verrucomicrobiae													1.15E-04
TOTAL	1.37E-03	4.19E-03	8.58E-06	1.07E-05	1.75E-03	2.15E-06	2.71E-02	1.84E-03	5.10E-03	6.93E-04	2.81E-03	1.96E-03	6.84E-01

Supplemental Table 3. Relative abundance of different autotrophy genes and their taxonomic assignment for Castle Chimney.

Taxa	*rbcS* (%)	*rbcL* (%)	*aclB* (%)	*cooS* (%)	*amoA* (%)	*nifH* (%)	*nirK* (%)	*dsrAB* (%)	*soxAB* (%)	*cyc2* (%)	*arsC* (%)	*ccoNO* (%)	*coxAB* (%)
Acidimicrobiia													4.24E-03
Acidithiobacillia		6.00E-04											
Acidobacteria		1.55E-05						1.03E-04					1.02E-03
Acidobacteriia													1.46E-04
Actinobacteria											9.71E-06		2.78E-03
Actinomycetia				5.83E-06									4.87E-05
Alphaproteobacteria		4.74E-04				3.30E-05	2.23E-04	1.23E-03	2.54E-03		4.08E-05		1.47E-02
Anaerolineae													2.92E-04
Ardenticatenia													1.53E-03
Bacteria	3.46E-03			3.89E-03		1.33E-03	7.19E-03	2.49E-04	1.03E-02		1.05E-04	1.39E-03	8.45E-02
Bacteroidetes							5.95E-04			6.29E-04	2.56E-04	1.13E-02	1.46E-04
Bacteroidia							6.80E-05						
Betaproteobacteria		3.44E-04			1.94E-05	1.55E-05	6.41E-05	4.45E-04	3.59E-04		6.02E-05		3.41E-04
Campylobacteria			7.77E-06						1.94E-06				4.87E-05
Candidatus Bipolaricaulota													4.87E-05
Candidatus Omnitrophica				1.94E-06									
Candidatus Tectomicrobia													2.44E-05
Chlorobia				3.89E-06									
Chloroflexi		2.78E-04											3.17E-03
Chloroflexia							1.94E-06						
Cyanobacteria		1.94E-05											
Cyanophyceae		1.94E-05				3.89E-06							
Cytophagia													4.87E-05
Deinococci													4.14E-04
Deltaproteobacteria				2.80E-04		2.56E-04	1.75E-05	2.68E-04	2.08E-04	4.66E-05	1.17E-05	1.22E-04	1.85E-03

Elusimicrobia		1.36E-05											
Euryarchaeota							1.17E-05						
Firmicutes						3.89E-06							
Flavobacteriia							3.69E-05				1.17E-05	1.46E-04	1.95E-04
Gammaproteobacteria		1.51E-02		1.40E-03	2.72E-05	5.07E-04	3.63E-04	2.46E-02	5.02E-03	1.04E-02	2.21E-03	4.12E-03	1.32E-01
Gemmatimonadetes		1.94E-06									1.75E-05		9.74E-05
Halobacteria							1.88E-04						
Holophagae													4.87E-05
Hydrogenophilalia		1.75E-05				1.94E-06							
Ignavibacteria										3.85E-04			
Methanopyri						1.94E-06							
Nitrososphaeria					7.77E-06		2.72E-05						4.63E-04
Nitrospinae							1.94E-06				2.72E-05		2.44E-05
Nitrospira			5.83E-06				3.89E-06						
Nitrospirae			3.11E-05	4.21E-03		1.24E-03		3.05E-03					6.94E-03
Planctomycetes				7.77E-06			1.55E-05					9.74E-05	1.32E-03
Planctomycetia											9.13E-05	9.74E-05	4.87E-04
Proteobacteria		1.08E-02		2.27E-04	7.77E-06	1.11E-02	3.42E-04	1.04E-02	2.86E-03	2.33E-05	3.42E-04		1.19E-01
Saprospiria													4.87E-05
Thaumarchaeota					7.77E-06		1.17E-05						
Verrucomicrobia												9.74E-05	
Zetaproteobacteria		1.94E-06											
TOTAL	3.46E-03	2.77E-02	4.47E-05		6.99E-05	1.45E-02	9.16E-03	4.03E-02	2.13E-02	1.15E-02	3.18E-03	1.73E-02	2.57E-01

Supplemental Table 4. Relative abundance of different autotrophy genes and their taxonomic assignment for Pagoda Chimney.

Taxa	*rbcS* (%)	*rbcL* (%)	*aclB* (%)	*cooS* (%)	*amoA* (%)	*nifH* (%)	*nirK* (%)	*dsrAB* (%)	*soxAB* (%)	*cyc2* (%)	*arsC* (%)	*ccoNO* (%)	*coxAB* (%)
Acidobacteria								1.48E-03			1.30E-04	5.21E-05	2.60E-05
Alphaproteobacteria		6.69E-06						1.34E-05	2.68E-05				4.17E-04
Anaerolineae											2.01E-05		5.94E-03
Aquificae			1.34E-05						1.00E-05				
Archaea		5.55E-04	1.07E-04	7.36E-05				5.02E-05					
Archaeoglobi		1.34E-05		1.34E-05				4.01E-05					
Armatimonadetes				3.01E-05									
Bacteria	1.46E-03		9.10E-04	1.20E-03		1.00E-05	1.08E-03	4.38E-03	1.94E-04	5.69E-05	6.76E-04	8.86E-03	2.56E-02
Bacteroidetes		6.69E-05					7.59E-04			6.69E-06	2.94E-03	4.26E-02	4.06E-03
Bacteroidia											1.34E-05	2.08E-03	2.60E-04
Betaproteobacteria													7.81E-05
Caldilineae		3.35E-06											2.34E-04
Calditrichae											5.35E-05		
Calditrichaeota											5.69E-05		
Campylobacteria			3.59E-03						1.03E-03		9.33E-04		4.71E-02
Candidatus Bipolaricaulota			1.96E-03						1.00E-05				
Candidatus Hydrogenedentes				3.35E-06									
Candidatus Korarchaeota				3.01E-05									
Candidatus Lokiarchaeota		6.68E-06											
Candidatus Peregrinibacteria		1.34E-05											
Candidatus Sumerlaeota											8.70E-05		
Candidatus Thermoplasmatota		6.02E-05											
Candidatus Woesarchaeota		3.01E-05											
Chitinophagia													1.56E-04
Chlorobi											3.35E-04	2.21E-03	1.59E-03
Chloroflexi		2.78E-04	9.03E-05	1.74E-03		1.67E-05	8.03E-05		6.69E-06				8.15E-03
Crenarchaeota		4.35E-05											

Cytophagia												2.84E-03	5.21E-05
Deinococci		3.35E-06											
Deltaproteobacteria		6.02E-05		3.75E-03		1.24E-04		1.58E-03	1.00E-05				1.67E-03
Euryarchaeota		1.34E-05		4.01E-05		1.00E-05							
Firmicutes				1.67E-05		1.67E-05					1.00E-05		
Flavobacteriia											1.07E-04	1.46E-03	
Gammaproteobacteria		5.35E-05		1.34E-05		3.35E-06		1.38E-03	2.68E-05	1.67E-05	1.10E-04		1.09E-03
Gemmatimonadetes								3.35E-06				2.34E-04	
Ignavibacteriae											4.35E-05	1.04E-04	
Methanomicrobia		4.35E-05		1.00E-05									
Methanopyri				4.62E-03		1.80E-03							
Nitrospinae													5.21E-05
Nitrospirae				6.69E-06		6.69E-06		6.69E-06					5.21E-05
Phycisphaerae													1.30E-04
Proteobacteria		3.58E-04		1.80E-03	1.00E-05	4.01E-05	6.69E-06	6.02E-05			1.47E-04		3.91E-04
Spirochaetes											4.01E-05		
Thermococci		8.10E-04		9.94E-04									
Thermodesulfobacteria				6.69E-06				2.01E-05					
Thermoplasmata			5.19E-04										
Thermoprotei		7.69E-05		9.37E-05									
Verrucomicrobia							4.35E-05					1.38E-03	1.12E-03
Verrucomicrobiae												4.17E-04	
TOTAL	1.46E-03	2.42E-03	6.67E-03	1.43E-02	1.00E-05	1.99E-03	1.93E-03	8.99E-03	1.29E-03	6.36E-05	5.52E-03	6.04E-02	9.71E-02

Supplemental Table 5. Relative abundance of different autotrophy genes and their taxonomic assignment for Snap-Snap Chimney.

Taxa	*rbcS* (%)	*rbcL* (%)	*aclB* (%)	*cooS* (%)	*amoA* (%)	*nifH* (%)	*nirK* (%)	*dsrAB* (%)	*soxAB* (%)	*cyc2* (%)	*arsC* (%)	*ccoNO* (%)	*coxAB* (%)
Acidimicrobiia											9.68E-06		1.26E-03
Acidithiobacillia		1.45E-05											
Acidobacteria								1.99E-04	4.84E-06		1.94E-05	2.64E-03	2.03E-03
Acidobacteriia													8.12E-05
Actinobacteria							2.66E-05				4.84E-06		8.12E-05
Actinomycetia													3.25E-04
Alphaproteobacteria		1.67E-03					1.62E-03	1.39E-03	2.79E-03	9.68E-06	6.17E-04		1.08E-01
Aquificae			2.42E-05						4.14E-04				7.63E-03
Archaea		3.63E-05	4.60E-05	1.45E-05									
Archaeoglobi		4.60E-05		9.68E-06		4.84E-06		3.87E-05					
Ardenticatenia							7.26E-06						
Bacteria	3.27E-04		4.84E-06	3.29E-04		6.05E-05	4.50E-04	6.46E-04	8.09E-04	9.76E-04	8.21E-04	2.76E-03	2.33E-02
Bacteroidetes							3.39E-04			7.19E-04	2.18E-04	2.48E-02	2.88E-03
Bacteroidia							1.91E-04		4.84E-06				
Betaproteobacteria		6.78E-05			4.84E-06		1.69E-05				2.18E-05		9.74E-04
Caldilineae													1.62E-04
Calditrichaeota									2.42E-06		9.68E-06		8.12E-05
Candidatus Bipolaricaulota									9.68E-06				
Candidatus Heimdallarchaeota		4.84E-06											8.12E-05
Candidatus Lambdaproteobacteria													2.43E-04
Candidatus Omnitrophica													8.12E-05
Candidatus Sumerlaeota											2.42E-05	4.06E-04	4.87E-04
Chitinophagia													4.06E-04
Chlorobi											9.68E-06	2.84E-03	8.93E-04
Chloroflexi		4.84E-06		1.45E-05								8.12E-05	2.84E-03
Cytophagia												3.25E-04	6.09E-04
Dehalococcoidia								4.84E-06					

Deinococci		3.14E-03					5.57E-05				9.93E-05		1.93E-02
Deltaproteobacteria				4.20E-03		1.12E-03	4.84E-06	4.15E-03	4.02E-04			8.12E-05	4.38E-03
Campylobacteria			2.36E-02						1.40E-02		1.11E-02		1.03E+00
Euryarchaeota		9.68E-06											8.12E-05
Flavobacteriia							7.75E-05				5.04E-04	3.11E-02	4.63E-02
Gammaproteobacteria		3.14E-03			3.39E-05		1.67E-04	3.45E-03	3.46E-03	2.64E-04	7.26E-04		1.14E-01
Ignavibacteriae											4.84E-06	8.12E-05	6.90E-04
Methanomicrobia		2.42E-06											
Nitrososphaeria							2.42E-05						7.30E-04
Nitrospinae													1.06E-03
Nitrospira							1.69E-05						
Nitrospirae			9.68E-06	1.33E-04				7.26E-05	7.75E-05				
Oligoflexia												8.12E-05	3.65E-04
Phycisphaerae												2.43E-04	5.68E-04
Planctomycetes											4.84E-06	9.74E-04	1.95E-03
Planctomycetia													2.35E-03
Proteobacteria		4.31E-03		2.66E-05		2.42E-06	2.16E-03	5.25E-04	1.34E-03		2.33E-03	3.65E-04	2.53E-02
Saprospiria													4.06E-05
Sphingobacteriia												8.12E-05	
Spirochaetia													8.12E-05
Thaumarchaeota							2.66E-05						1.62E-04
Thermococci		1.45E-05											
Thermodesulfobacteria				9.44E-05		2.18E-05		1.14E-04					
Thermoprotei		1.45E-05											
Thermotogae							4.84E-06						8.12E-05
Verrucomicrobia							1.45E-05				2.18E-05		3.25E-04
Verrucomicrobiae							4.84E-06						8.12E-05
Zetaproteobacteria		1.14E-03					2.32E-04				6.15E-04	6.49E-04	1.15E-02
TOTAL	3.27E-04	1.25E-02	2.37E-02	4.73E-03	4.84E-06	1.19E-03	5.19E-03	1.05E-02	2.20E-02	1.70E-03	1.65E-02	6.68E-02	1.40E+00

Supplemental Table 6. Relative abundance of different autotrophy genes and their taxonomic assignment for Ultra-No-Chi-Chi Chimney.

Taxa	*rbcS* (%)	*rbcL* (%)	*aclB* (%)	*cooS* (%)	*amoA* (%)	*nifH* (%)	*nirK* (%)	*dsrAB* (%)	*soxAB* (%)	*cyc2* (%)	*arsC* (%)	*ccoNO* (%)	*coxAB* (%)
Acidithiobacillia		2.36E-05											
Acidimicrobiia											5.23E-06		8.43E-05
Acidobacteria								4.58E-04	5.23E-06		4.45E-05	8.18E-03	7.55E-03
Acidobacteriia													8.43E-05
Actinobacteria													1.26E-04
Actinomycetia											2.62E-06		
Alphaproteobacteria		3.82E-03						4.10E-03	6.26E-03		1.42E-03		9.64E-02
Anaerolineae													4.34E-03
Aquificae			8.27E-04	9.92E-04					1.86E-03	1.31E-05			1.99E-02
Archaea		4.03E-04	5.23E-06	9.16E-05									7.17E-04
Archaeoglobi		6.52E-04		1.15E-04		1.02E-04		1.38E-03					3.37E-04
Armatimonadetes				2.62E-06									
Bacteria	1.54E-04		1.57E-04	6.67E-04		1.15E-04	2.38E-04	1.51E-03	1.89E-03		1.73E-03	3.38E-02	9.16E-02
Bacteroidetes							1.78E-04				3.64E-04	7.80E-03	1.55E-02
Betaproteobacteria		1.05E-04											
Caldilineae								1.05E-05					1.35E-03
Calditrichae	3.66E-05												9.70E-04
Calditrichaeota		3.40E-05									1.02E-04		9.28E-04
Candidatus Bathyarchaeota				3.66E-05									
Candidatus Bipolaricaulota									2.36E-05				
Candidatus Heimdallarchaeota		3.32E-04											3.25E-03
Candidatus Hydrogenedentes													4.22E-04
Candidatus Marinimicrobia													9.28E-04
Candidatus Microgenomates		5.23E-06											
Candidatus Pacearchaeota		1.57E-05											
Candidatus Sumerlaeota											5.76E-05	2.70E-03	1.22E-03
Chitinophagia													1.69E-04
Chlorobi											5.76E-05	1.45E-02	1.26E-02
Chloroflexi		1.05E-05		3.93E-05			1.62E-04					6.75E-04	3.60E-02

Cytophagia													8.43E-04
Deinococci		3.00E-04					1.31E-04				2.04E-04		5.00E-02
Deltaproteobacteria				1.68E-03		5.50E-05		1.50E-03	2.36E-05			1.48E-03	1.05E-02
Epsilonproteobacteria			1.97E-02						1.22E-02		1.22E-02		8.69E-01
Euryarchaeota		2.62E-05		3.14E-05				1.05E-05					2.40E-03
Flavobacteriia							2.43E-04				3.30E-04	2.00E-02	2.96E-02
Gammaproteobacteria		1.48E-03					8.64E-05	3.17E-03	5.85E-03		2.26E-03		1.32E-01
Halobacteria													4.22E-05
Ignavibacteriae											4.71E-05	8.01E-04	3.42E-03
Methanomicrobia				1.57E-05									
Nitrososphaeria													3.37E-04
Nitrospinae			1.05E-05						7.33E-05				4.22E-04
Nitrospirae				1.46E-03		3.66E-05		1.04E-03	5.99E-04				
Oligoflexia												8.01E-04	3.37E-04
Planctomycetes							3.40E-05					7.38E-03	7.17E-03
Planctomycetia													2.53E-04
Proteobacteria		1.06E-02		4.71E-05		2.62E-06	2.54E-04	7.24E-04	1.75E-04	8.64E-05		4.22E-04	1.82E-02
Saprospira		2.62E-06										4.22E-05	1.69E-04
Spirochaetes													3.37E-04
Spirochaetia							2.62E-05						1.94E-03
Thaumarchaeota													1.69E-04
Thermococci		4.19E-05		1.81E-04									
Thermodesulfobacteria				2.17E-04		2.62E-05		2.38E-04					
Thermomicrobia													1.26E-04
Thermoprotei		2.41E-04		2.62E-05									
Thermotogae							4.97E-05						5.14E-03
Verrucomicrobia												4.22E-05	
Zetaproteobacteria		3.64E-04					1.67E-04					1.26E-04	5.57E-03
TOTAL	1.91E-04	1.85E-02	2.07E-02	5.60E-03		3.37E-04	1.57E-03	1.41E-02	2.90E-02	9.95E-05	1.88E-02		1.43E+00

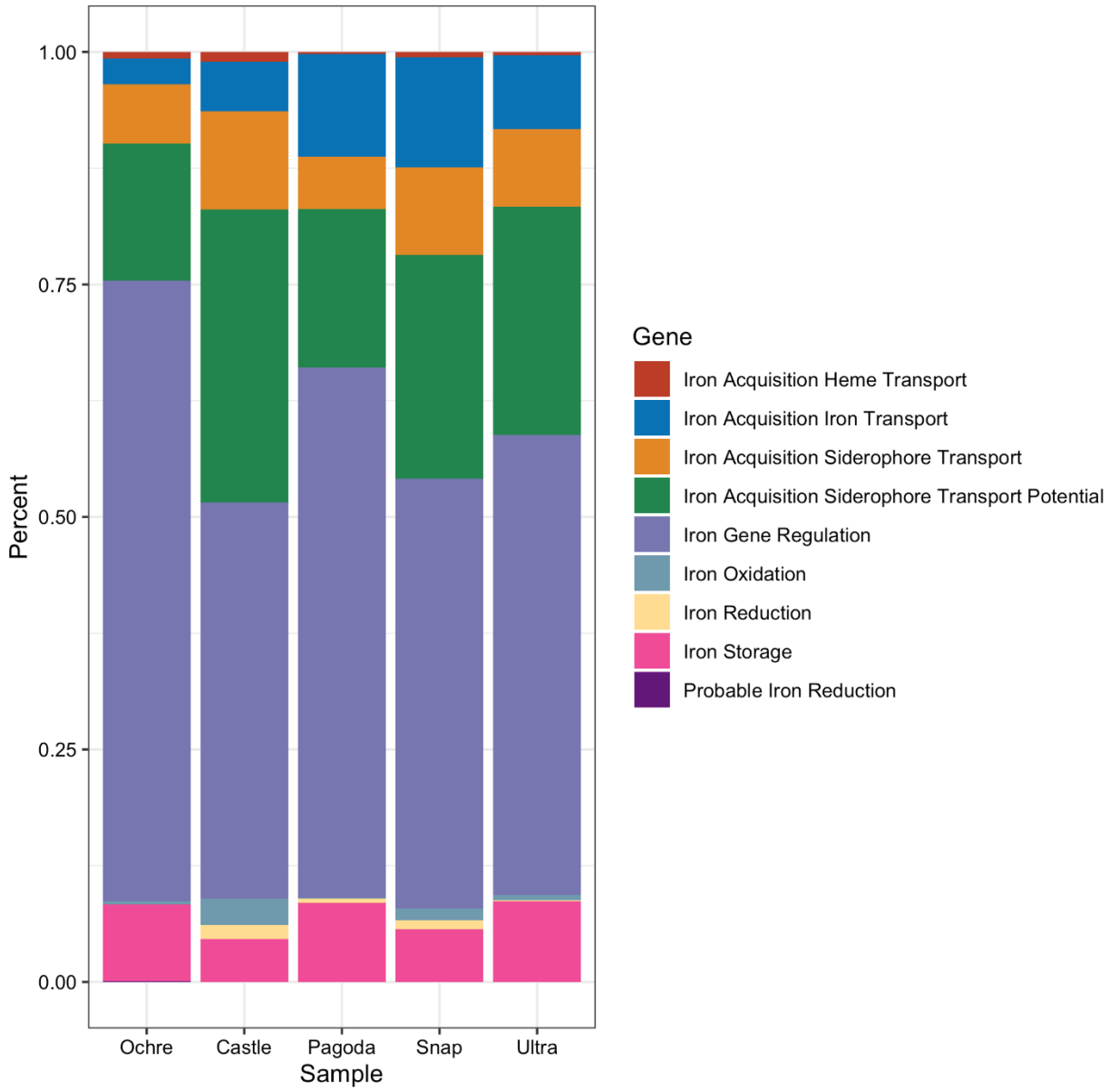

Supplemental Figure 1. Stacked bar graph as a percentage of the whole of different types of iron genes found in each chimney from the FeGenie analysis.